به نام خدا

مرکز دانلود رایگان
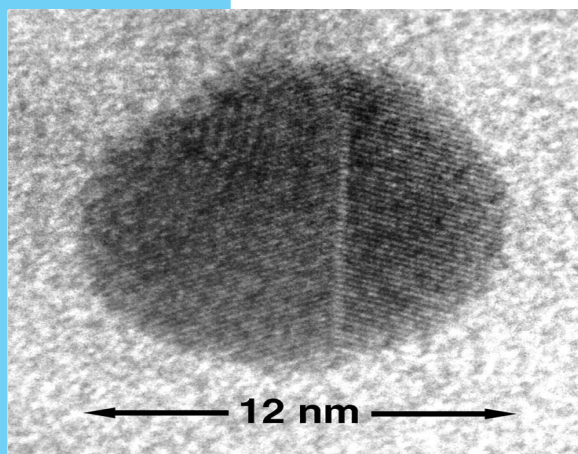# مهندسی متالورژی و مواد

www.Iran-mavad.com

CHAPTER **4**
Crystal Defects and Noncrystalline Structure— Imperfection

As with the chapter-opening photograph for Chapter 3, this transmission electron micrograph provides an atomic-resolution image of a crystalline compound, viz. a small crystal of zinc selenide embedded in a glass matrix. By viewing individual crystal lattice planes in ZnSe, we can see a distinctive image of a vertical twin boundary (shown schematically in Figure 14–15). This ZnSe "quantum dot" is the basis of a blue light laser. (Courtesy of V. J. Leppert and S. H. Risbud, University of California, Davis and M. J. Fendorf, National Center for Electron Microscopy, Berkeley, California.)
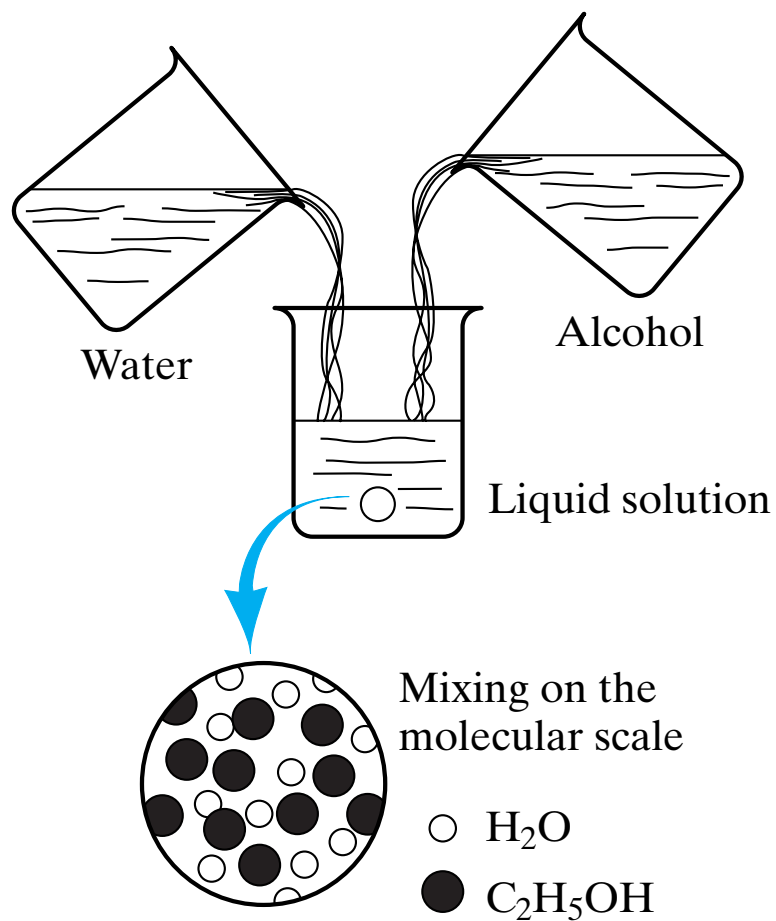
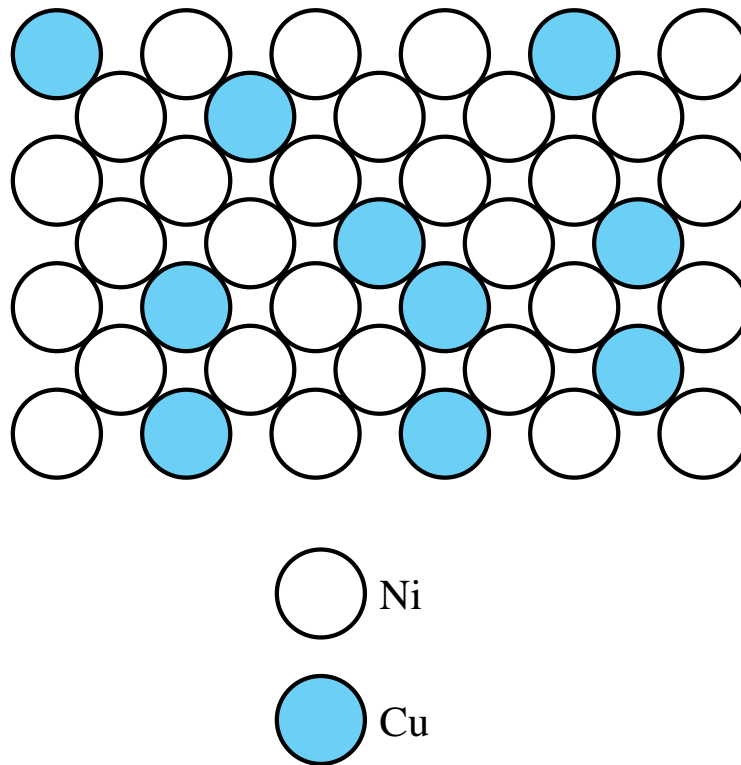**Figure 4-1** *Forming a liquid solution of water and alcohol. Mixing occurs on the molecular scale.*

Figure 4-2 *Solid solution of copper in nickel shown along a (100) plane. This is a* sub-stitutional *solid solution with nickel atoms substituting for copper atoms on fcc atom sites.*
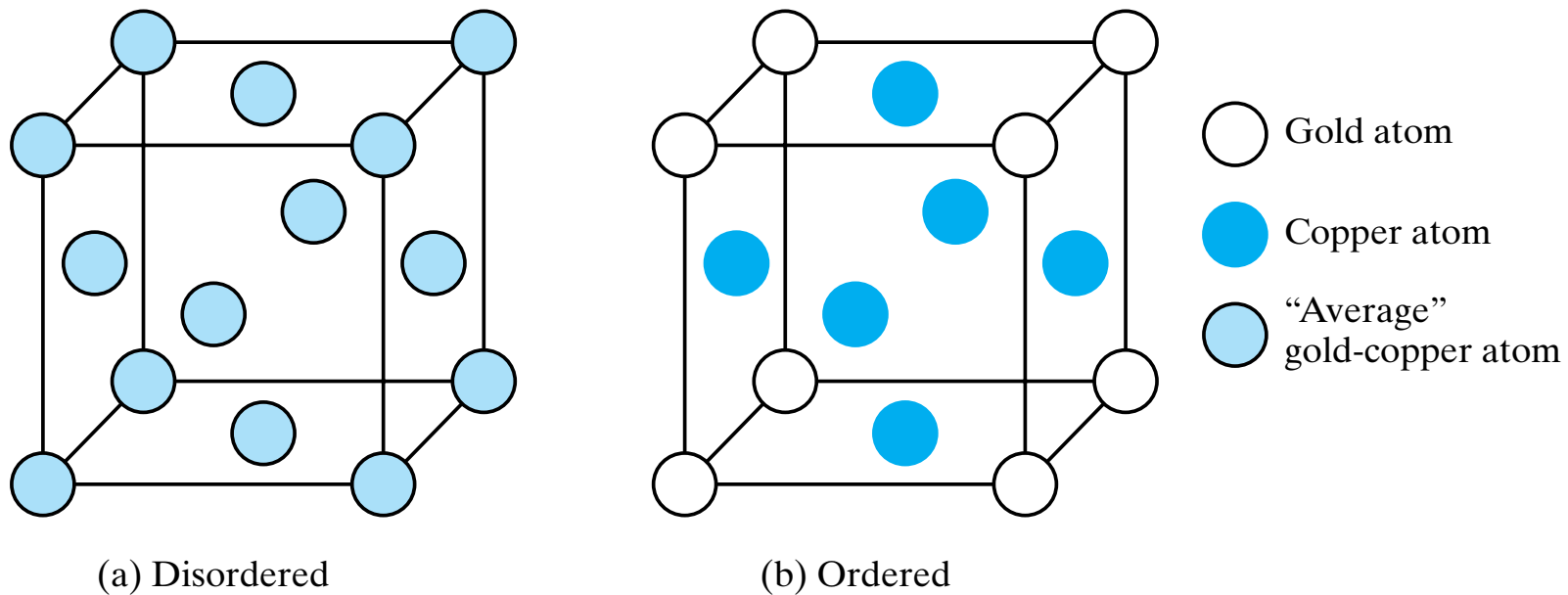
(a) Disordered (b) Ordered

Legend:
○ Gold atom
● Copper atom
◔ "Average" gold-copper atom

Figure 4-3 *Ordering of the solid solution in the AuCu₃ alloy system. (a) Above ∼ 390°C, there is a random distribution of the Au and Cu atoms among the fcc sites. (b) Below ∼ 390°C, the Au atoms preferentially occupy the corner positions in the unit cell, giving a simple cubic Bravais lattice. (From B. D. Cullity,* Elements of X-Ray Diffraction, *2nd ed., Addison-Wesley Publishing Co., Inc., Reading, Mass., 1978.)*
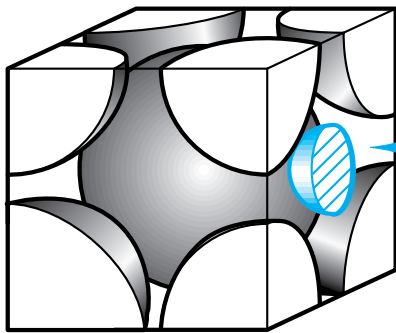
C atom dissolved interstitially at a $\frac{1}{2}$ 0 $\frac{1}{2}$-type position in the bcc structure of α-Fe

Figure 4-4 *Interstitial solid solution of carbon in α-iron. The carbon atom is small enough to fit with some strain in the interstice (or opening) among adjacent Fe atoms in this structure of importance to the steel industry. [This unit cell structure can be compared with Figure 3–4b.]*
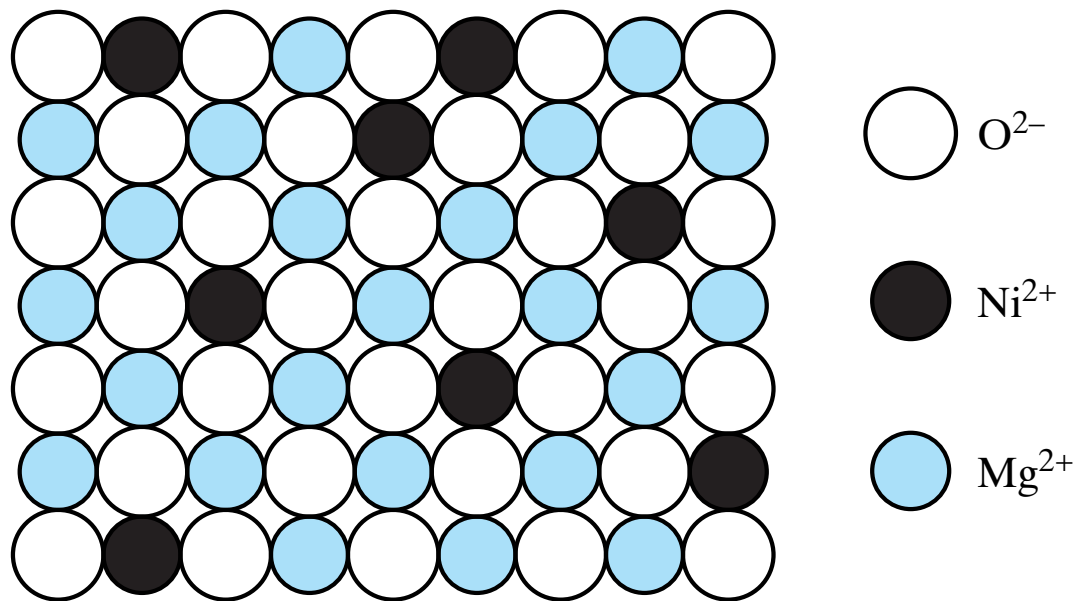
Figure 4-5 *Random, substitutional solid solution of NiO in MgO. The O^{2-} arrangement is unaffected. The substitution occurs among Ni^{2+} and Mg^{2+} ions.*
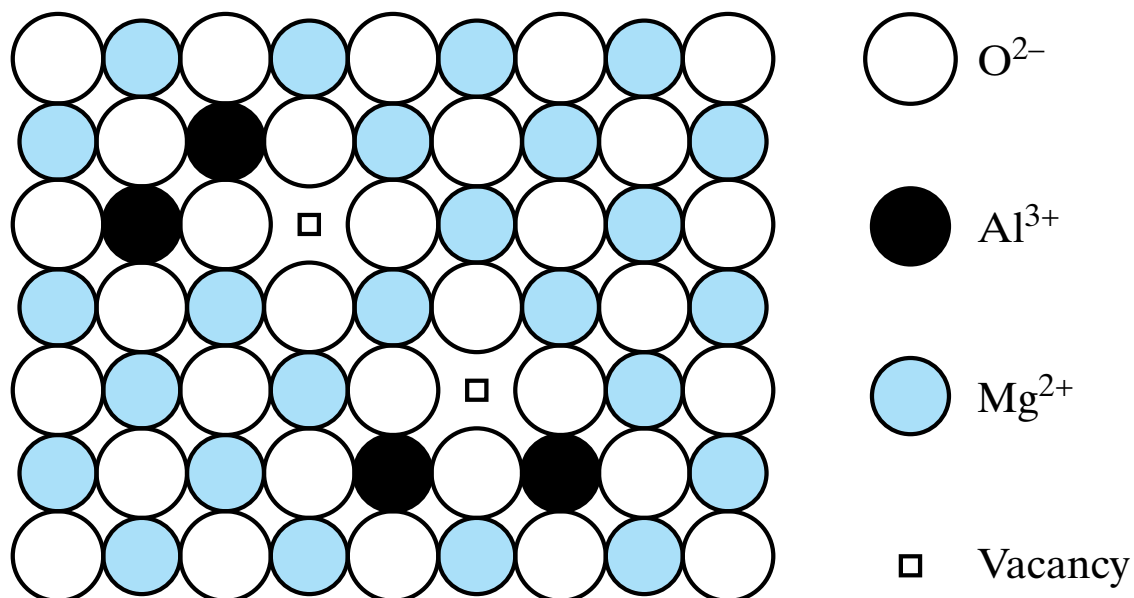
Figure 4-6 *A substitutional solid solution of Al_2O_3 in MgO is not as simple as the case of NiO in MgO (Figure 4–5). The requirement of charge neutrality in the overall compound permits only two Al^{3+} ions to fill every three Mg^{2+} vacant sites, leaving one Mg^{2+} vacancy.*
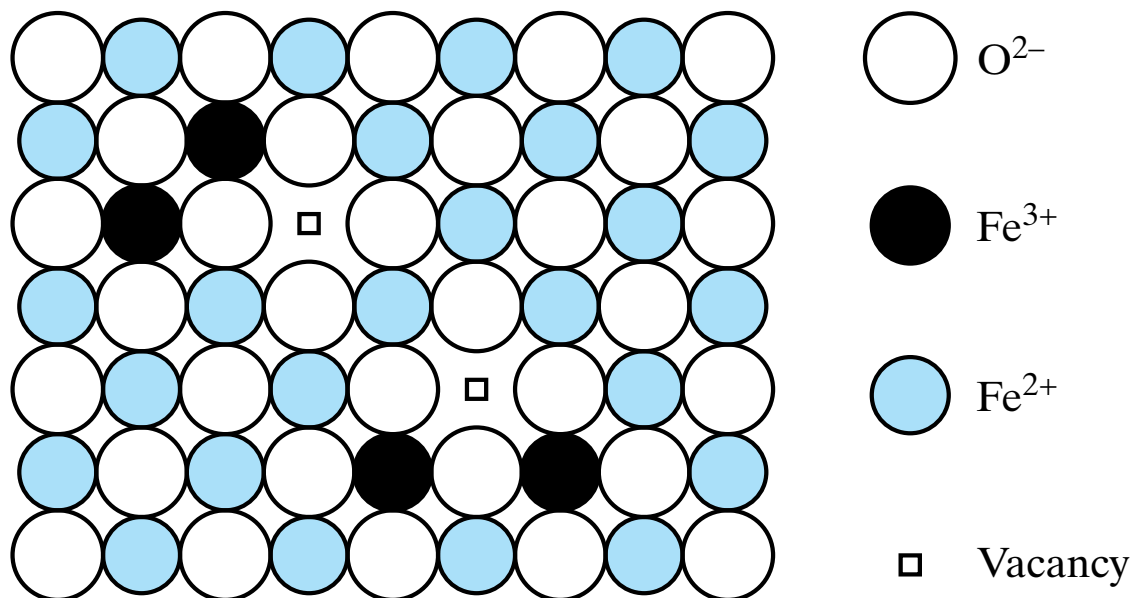
Figure 4-7 *Iron oxide, $Fe_{1-x}O$ with $x \approx 0.05$, is an example of a nonstoichiometric compound. Similar to the case of Figure 4–6, both Fe^{2+} and Fe^{3+} ions occupy the cation sites with one Fe^{2+} vacancy occurring for every two Fe^{3+} ions present.*
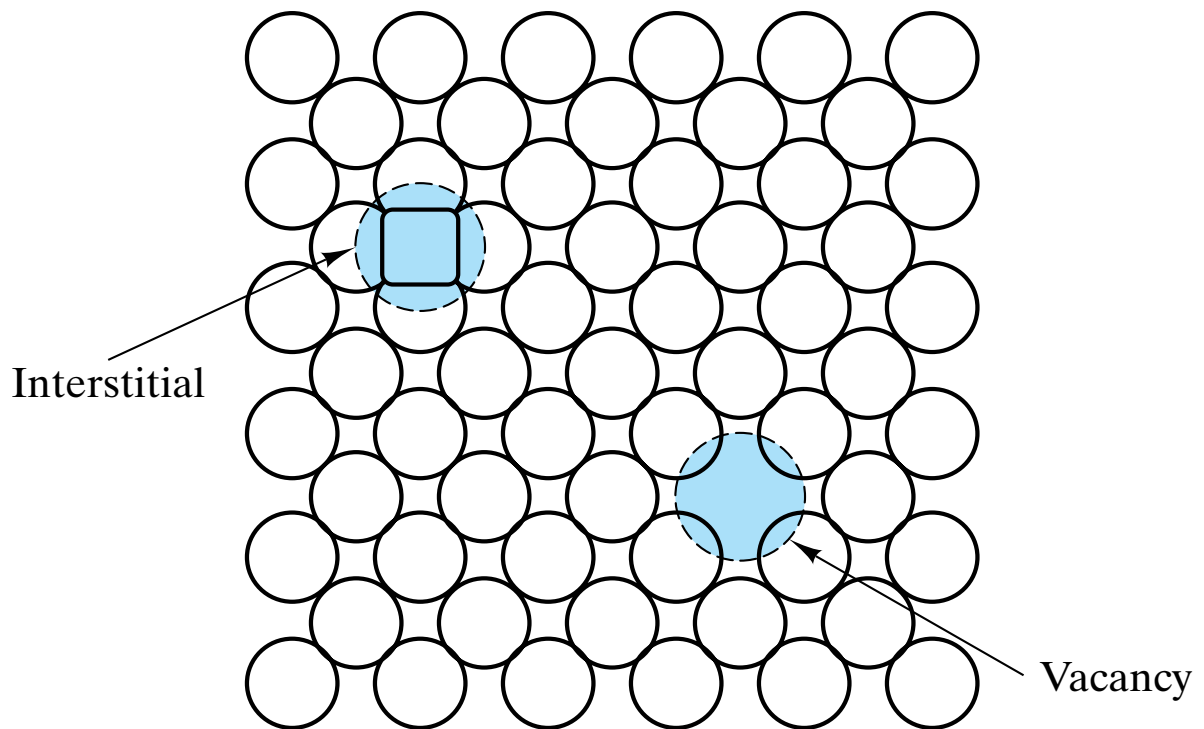
Figure 4-8 *Two common point defects in metal or elemental semiconductor structures are the vacancy and the interstitial.*
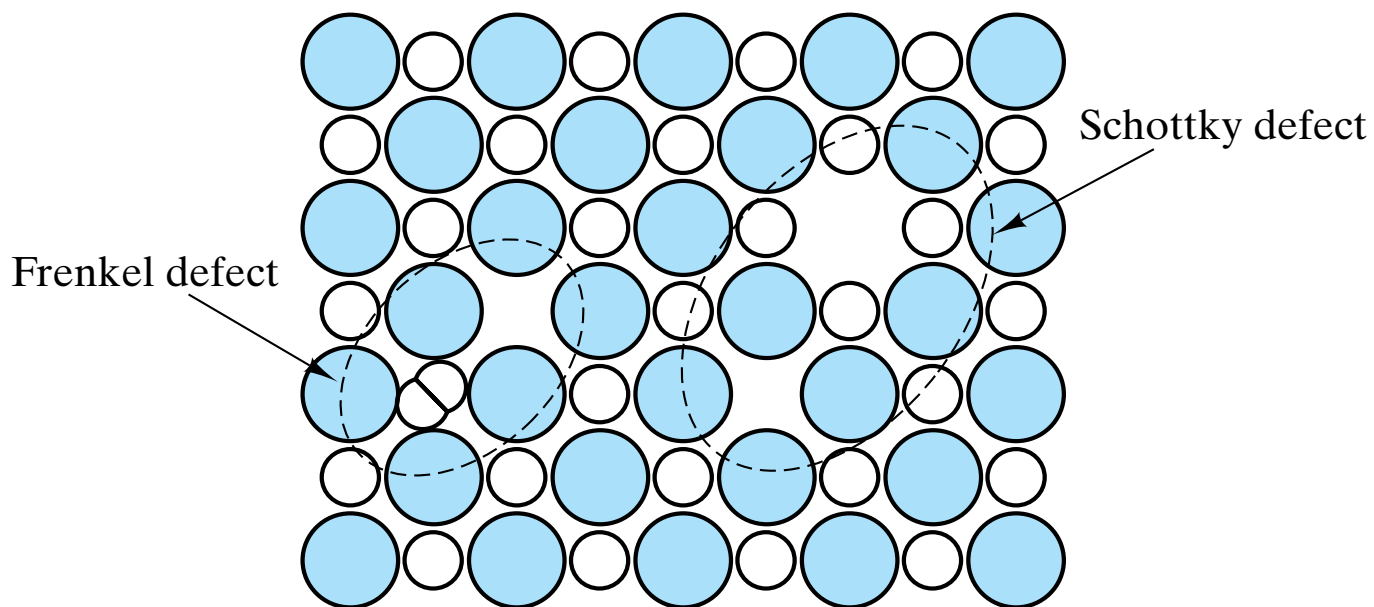
Figure 4-9 *Two common point defect structures in compound structures are the Schottky defect and the Frenkel defect. Note their similarity to the structures of Figure 4–8.*
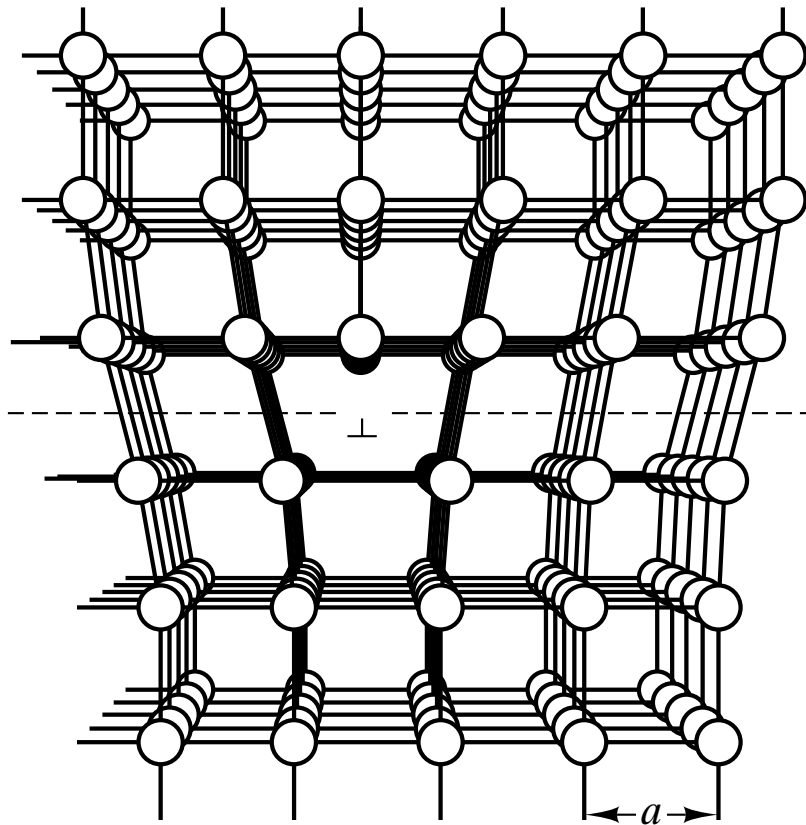
Figure 4-10 *Edge dislocation. The linear defect is represented by the edge of an extra half-plane of atoms. (From A. G. Guy,* Elements of Physical Metallurgy, *Addison-Wesley Publishing Co., Inc., Reading, Mass., 1959.)*

Figure 4-11 *Definition of the Burgers vector,* **b,** *relative to an edge dislocation. (a) In the perfect crystal, an m × n atomic step loop closes at the starting point. (b) In the region of a dislocation, the same loop does not close, and the closure vector* **(b)** *represents the magnitude of the structural defect. For the edge dislocation, the Burgers vector is* perpendicular *to the dislocation line.*
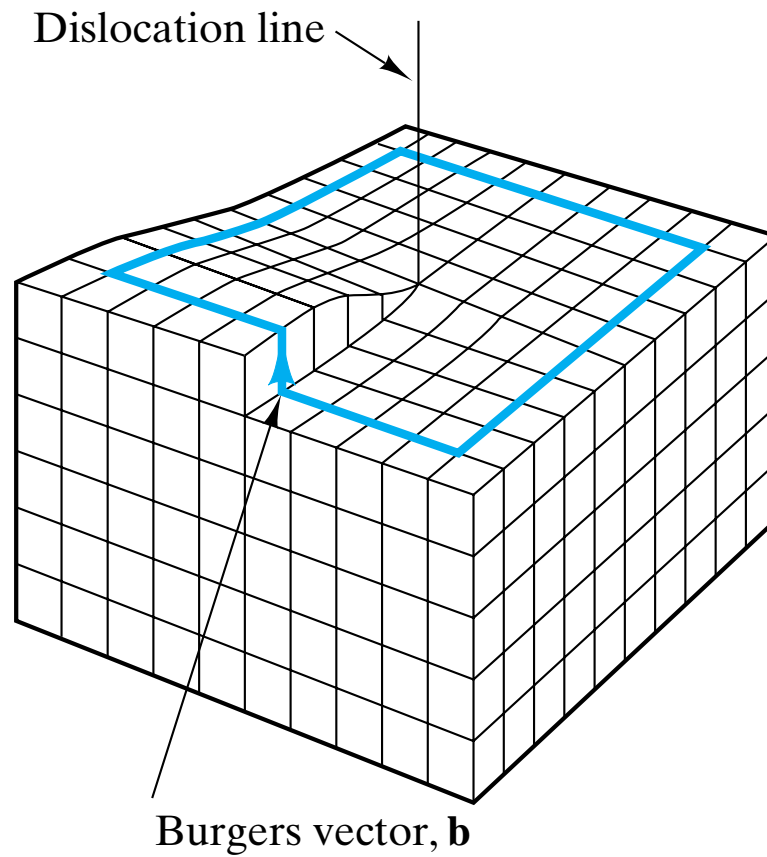
(a)

(b)

Dislocation line
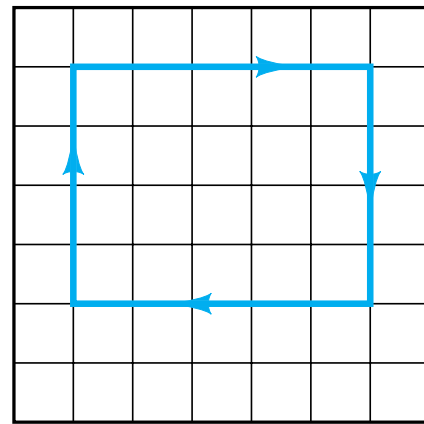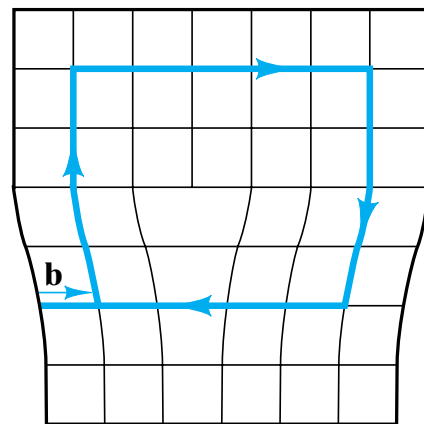
Burgers vector, **b**

Figure 4-12 *Screw dislocation. The spiral stacking of crystal planes leads to the Burgers vector being* parallel *to the dislocation line.*
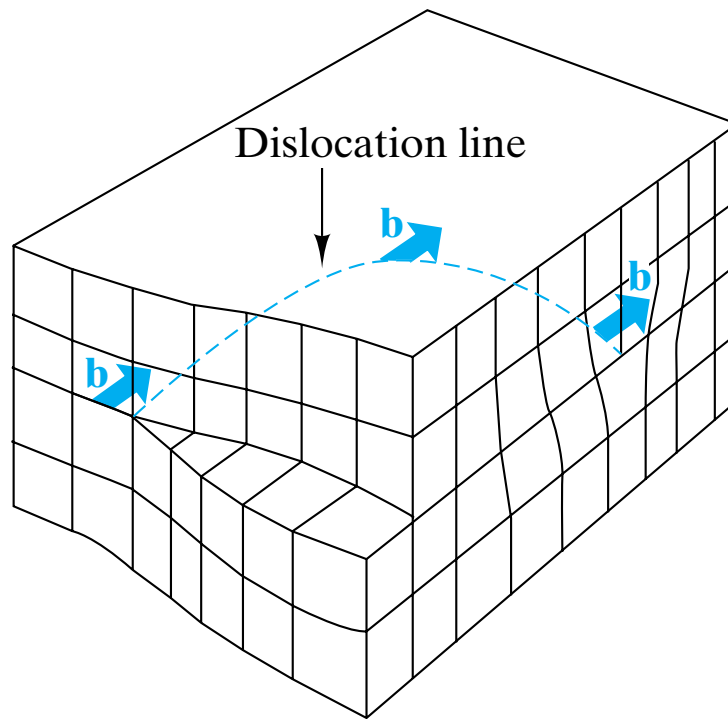
Figure 4-13 *Mixed dislocation. This has both edge and screw character with a single Burgers vector consistent with the pure edge and pure screw regions.*
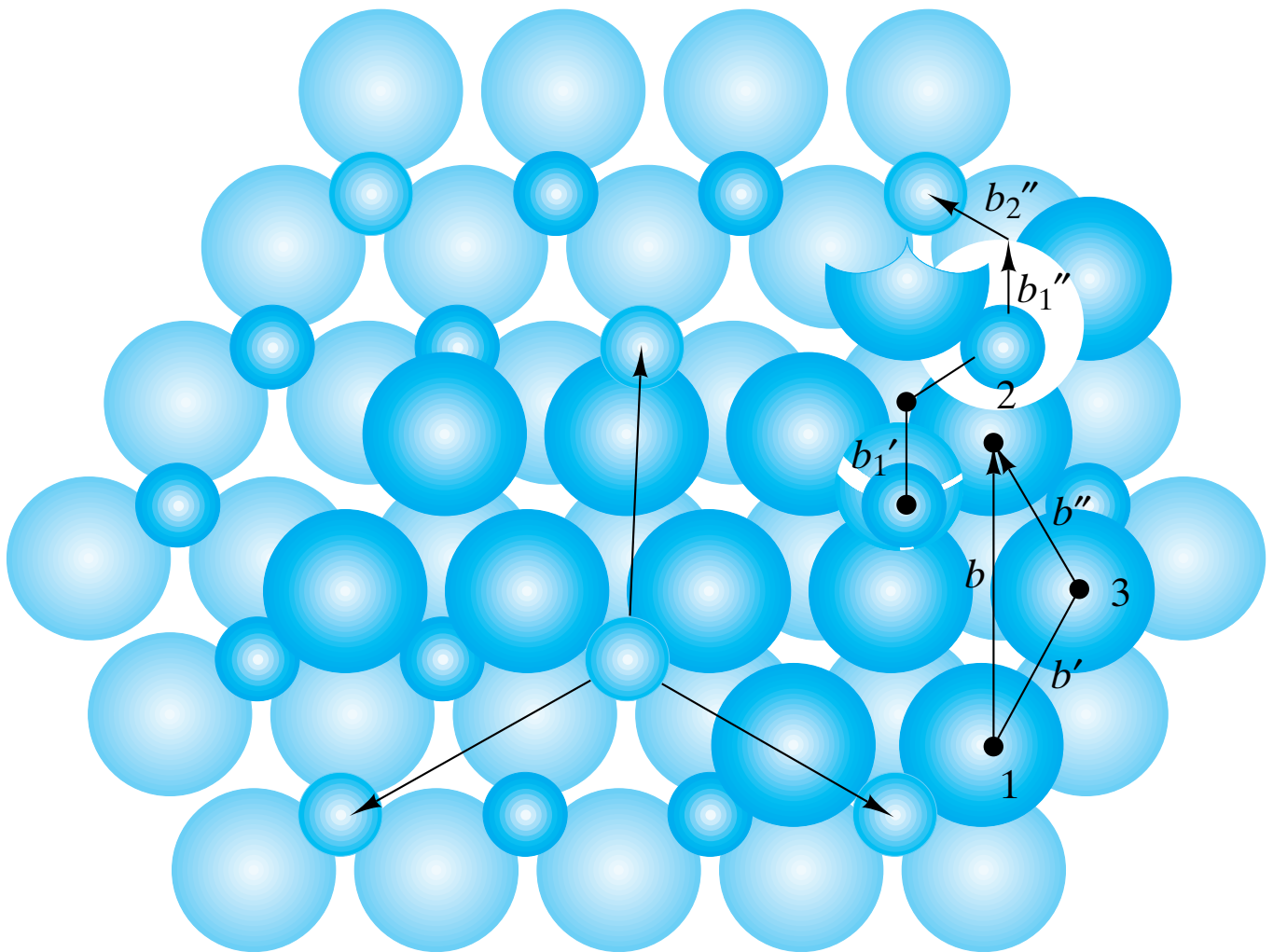
Figure 4-14 *Burgers vector for the aluminum oxide structure. The large repeat distance in this relatively complex structure causes the Burgers vector to be broken up into two (for O^{2-}) or four (for Al^{3+}) partial dislocations, each representing a smaller slip step. This complexity is associated with the brittleness of ceramics compared to metals. (From W. D. Kingery, H. K. Bowen, and D. R. Uhlmann,* Introduction to Ceramics, *2nd ed., John Wiley & Sons, Inc., New York, 1976.)*
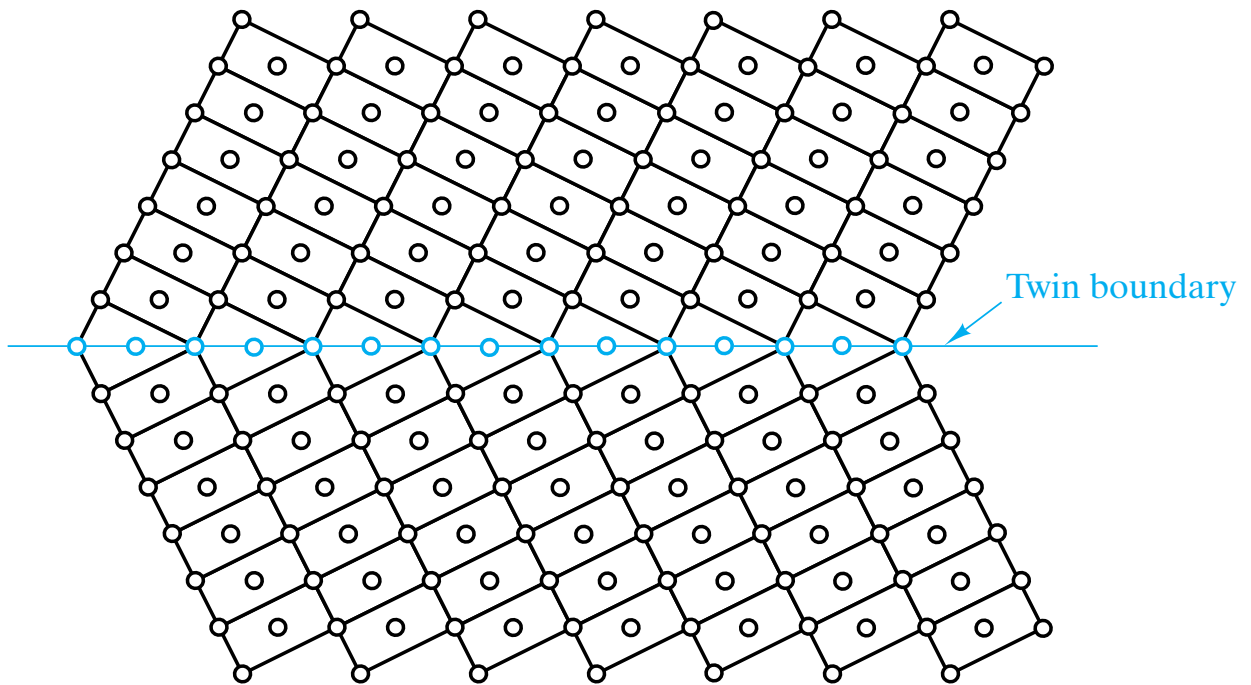
30°

2

1
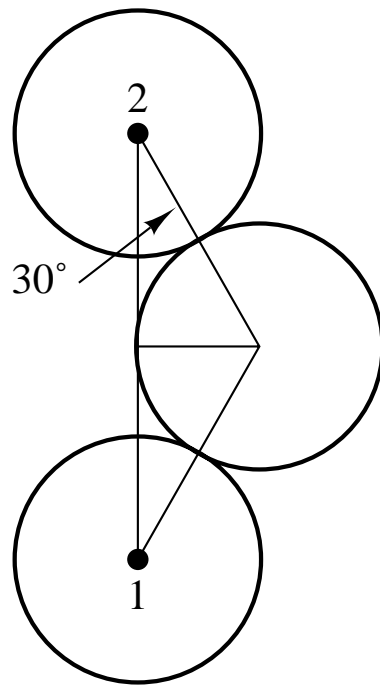
Figure 4-15 *A twin boundary separates two crystalline regions that are, structurally, mirror images of each other.*
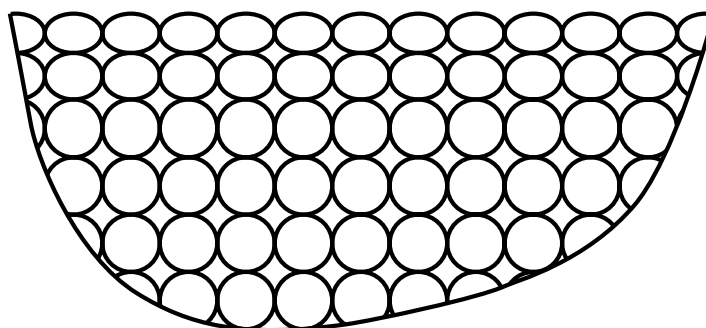
Figure 4-16 *Simple view of the surface of a crystalline material.*
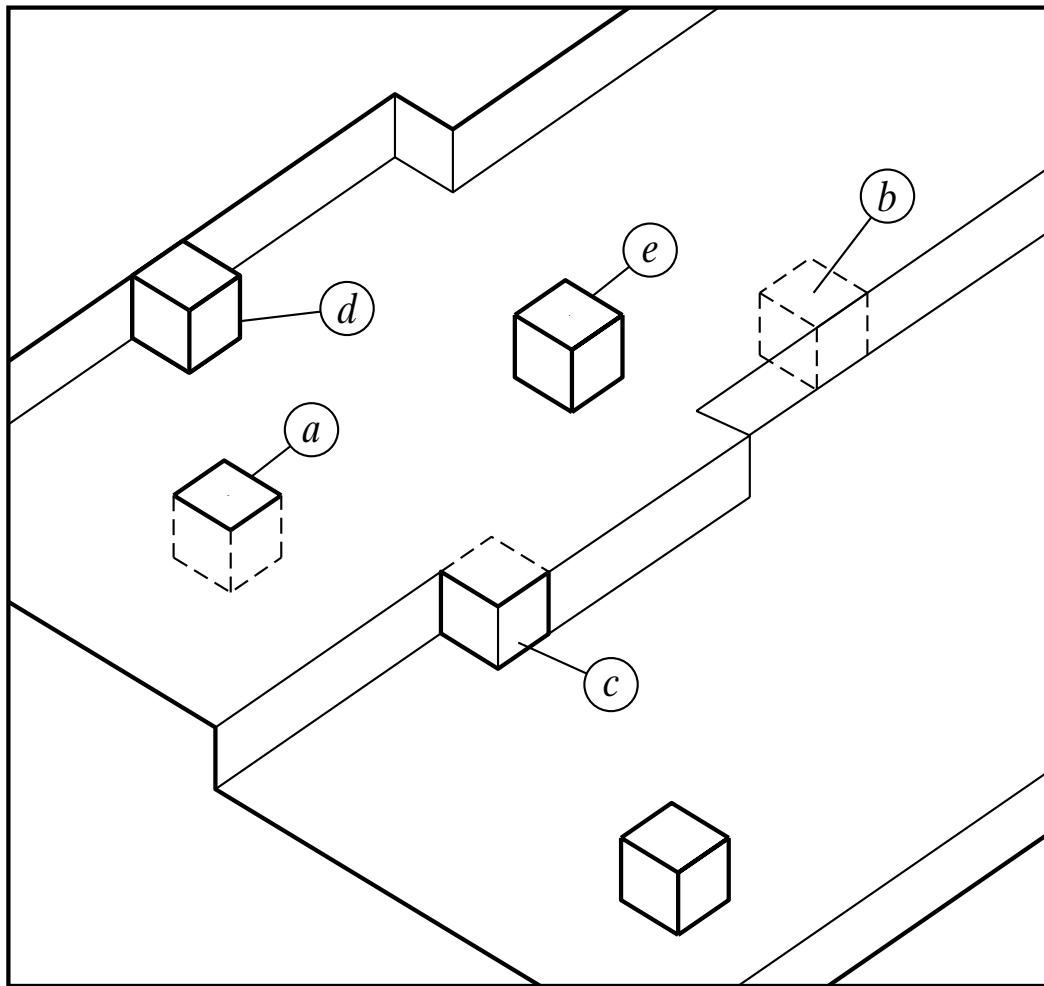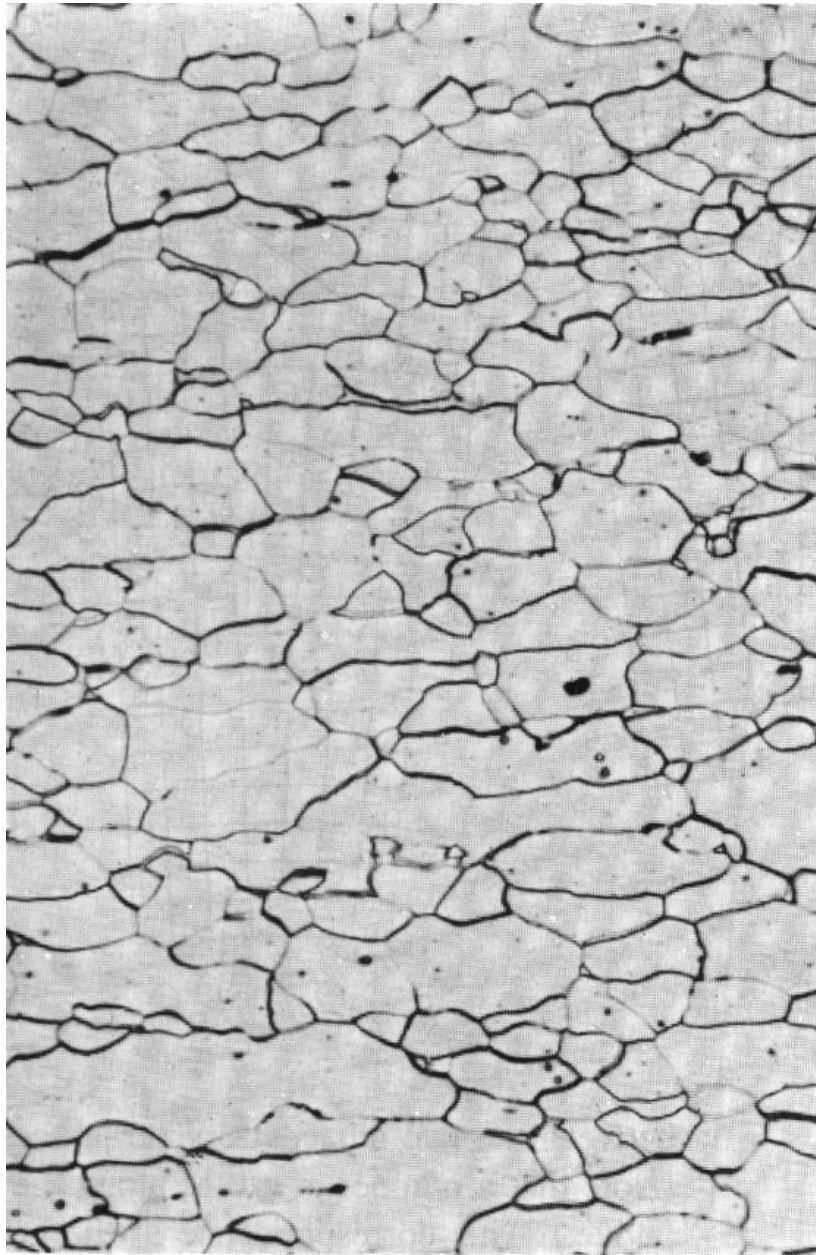
Figure 4-17 *A more detailed model of the elaborate ledgelike structure of the surface of a crystalline material. Each cube represents a single atom. [From J. P. Hirth and G. M. Pound,* J. Chem. Phys. 26, *1216 (1957).]*

Nital   100×

Figure 4-18 *Typical optical micrograph of a grain structure, 100×. The material is a low-carbon steel. The grain boundaries have been lightly etched with a chemical solution so that they reflect light differently from the polished grains, thereby giving a distinctive contrast. (From* Metals Handbook, *8th ed., Vol. 7:* Atlas of Microstructures of Industrial Alloys, *American Society for Metals, Metals Park, Ohio, 1972.)*
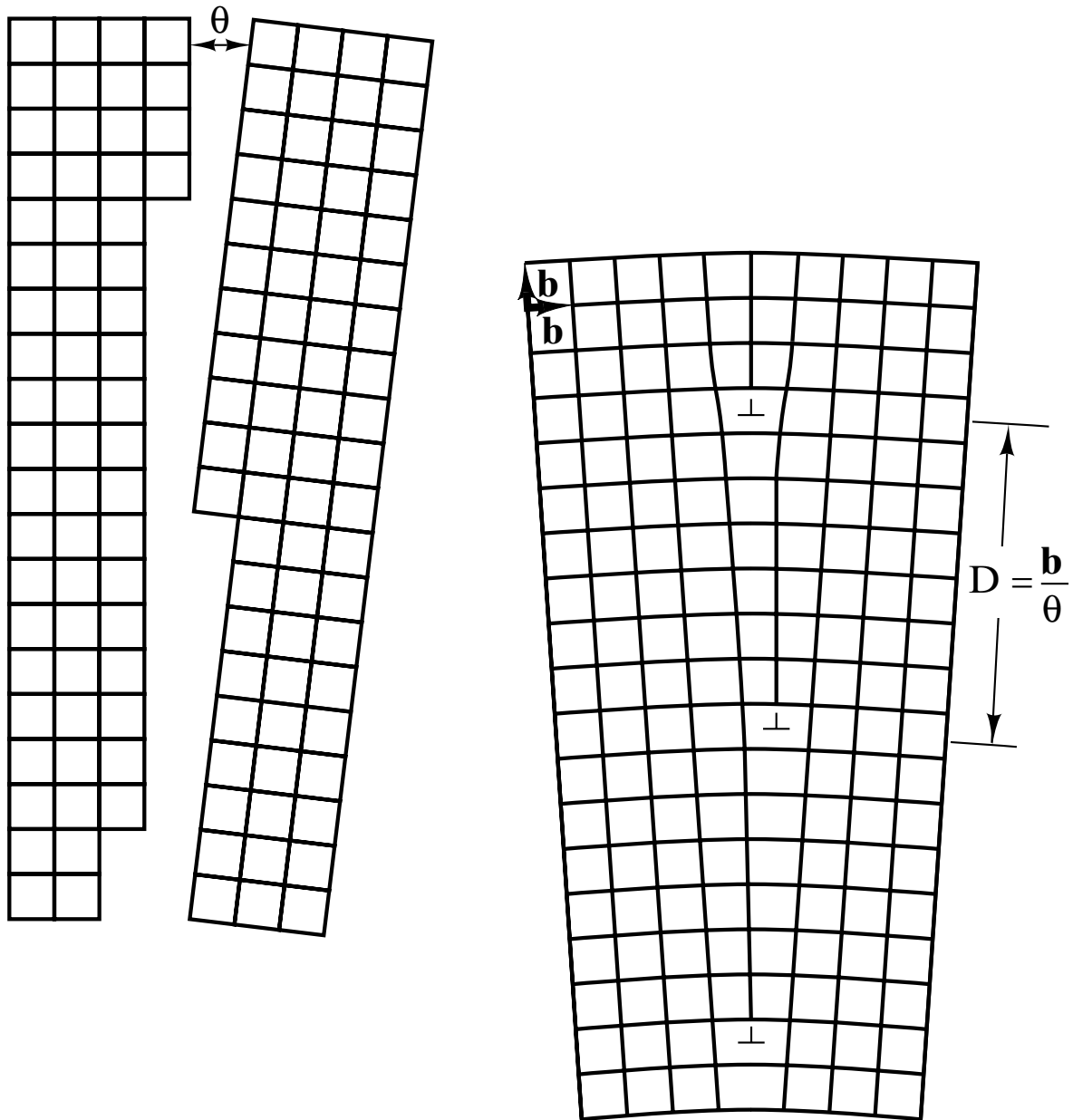
Figure 4-19 *Simple grain boundary structure. This is termed a tilt boundary because it is formed when two adjacent crystalline grains are tilted relative to each other by a few degrees (θ). The resulting structure is equivalent to isolated edge dislocations separated by the distance b/θ, where b is the length of the Burgers vector,* **b.** *(From W. T. Read,* Dislocations in Crystals, *McGraw-Hill Book Company, New York, 1953. Reprinted with permission of the McGraw-Hill Book Company.)*
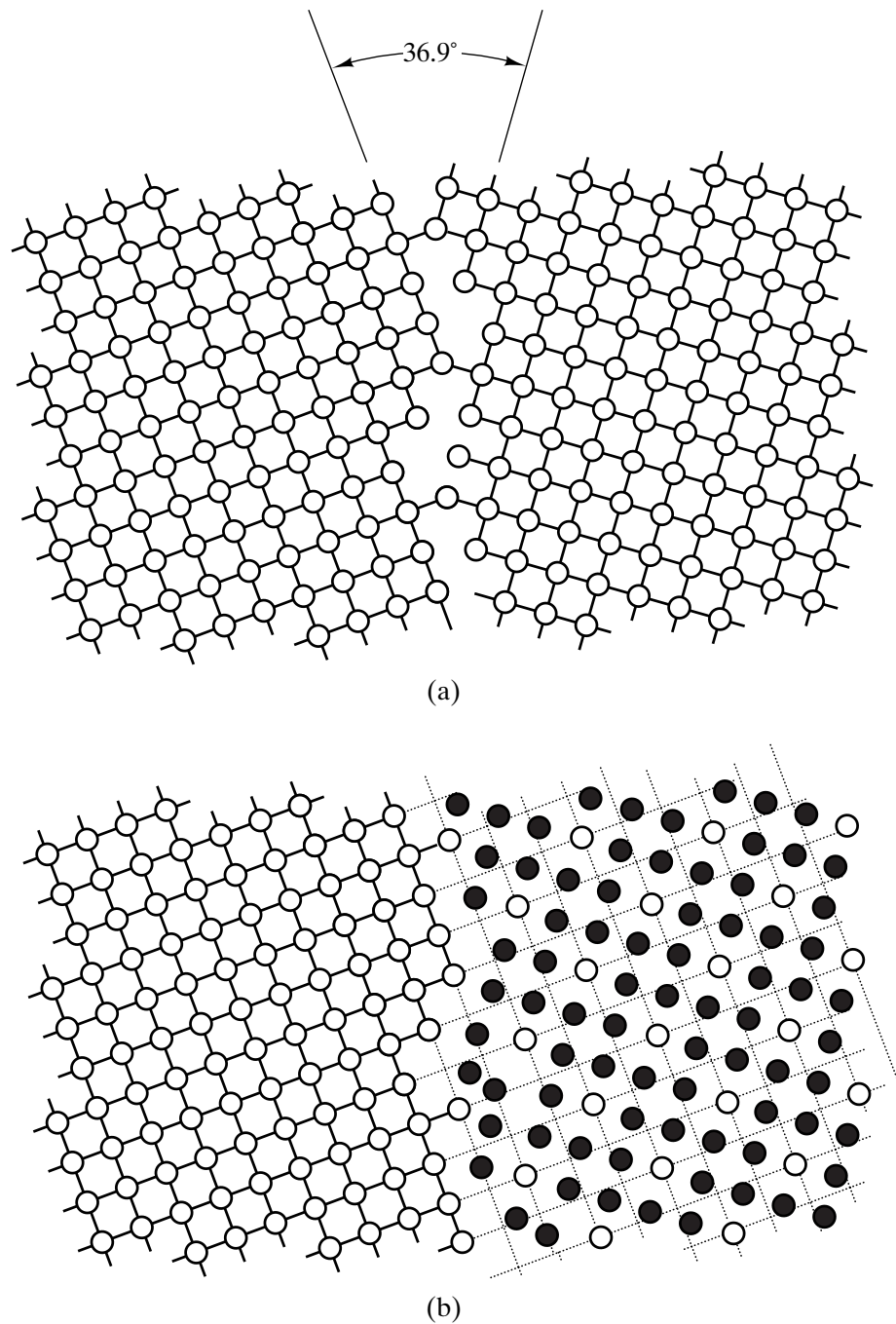
Figure 4-20 *(a) A high-angle ($\theta = 36.9°$) grain boundary between two square lattice grains can be represented by a coincidence site lattice, as shown in (b). As one in five of the atoms in the grain on the right is coincident with the lattice of the grain on the left, the boundary is said to have $\Sigma^{-1} = 1/5$, or $\Sigma = 5$.*
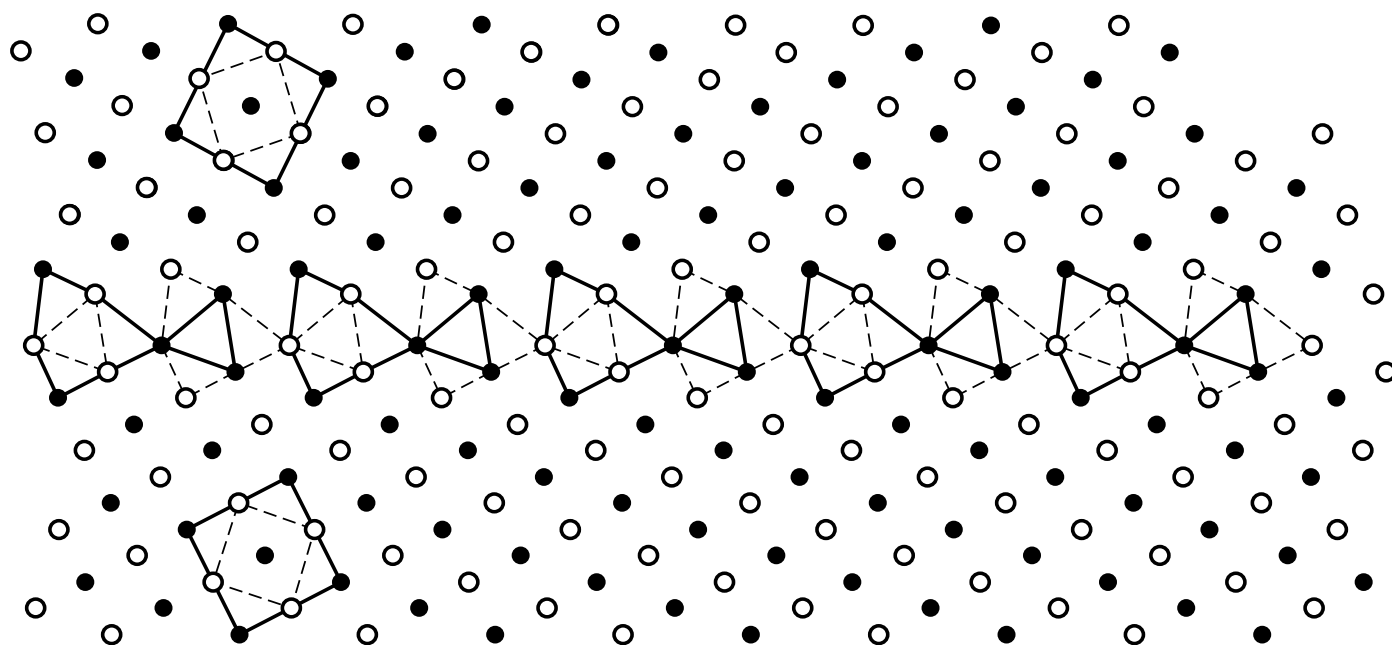
Figure 4-21 *A Σ5 boundary for an fcc metal, in which the [100] directions of two adjacent fcc grains are oriented at 36.9° to each other. (See Figure 4–20 also.) This is a three-dimensional projection with the open circles and closed circles representing atoms on two different, adjacent planes (each parallel to the plane of this page). Polyhedra formed by drawing straight lines between adjacent atoms in the grain boundary are irregular in shape due to the misorientation angle, 36.9°, but reappear at regular intervals due to the crystallinity of each grain. The crystalline grains can be considered to be composed completely of tetrahedra and octahedra.* [Reprinted with permission from M. F. Ashby, F. Spaepen, and S. Williams, Acta Metall. 26, 1647 (1978), Copyright 1978, Pergamon Press, Ltd.]
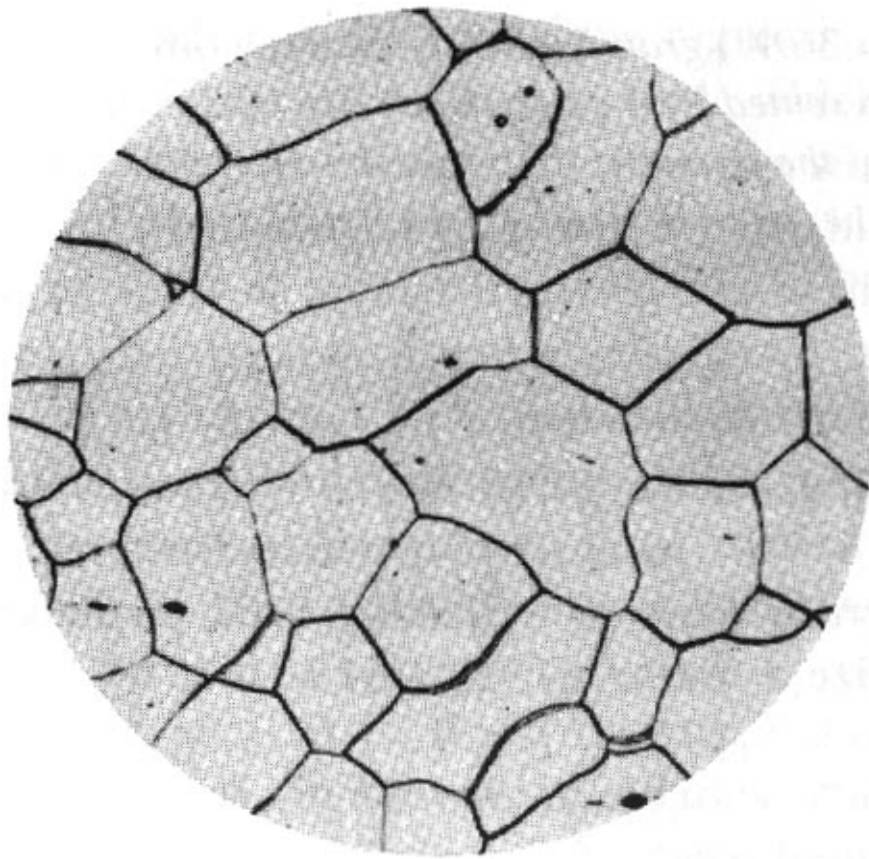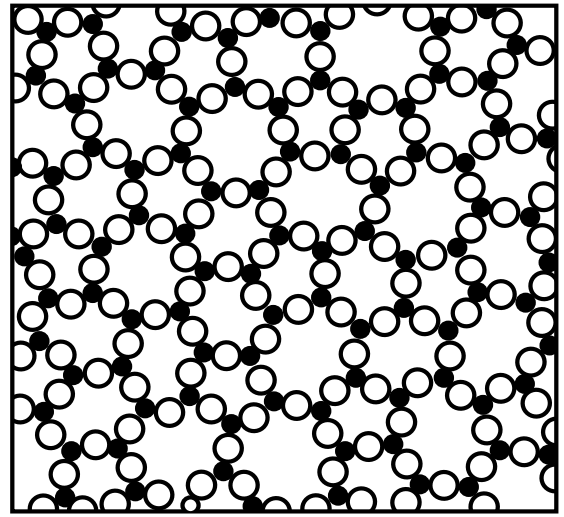
Nital   100×

Figure 4-22 *Specimen for the calculation of the grain-size number, G, 100×. The material is a low-carbon steel similar to that shown in Figure 4–18. (From* Metals Handbook, *8th ed., Vol. 7:* Atlas of Microstructures of Industrial Alloys, *American Society for Metals, Metals Park, Ohio, 1972.)*
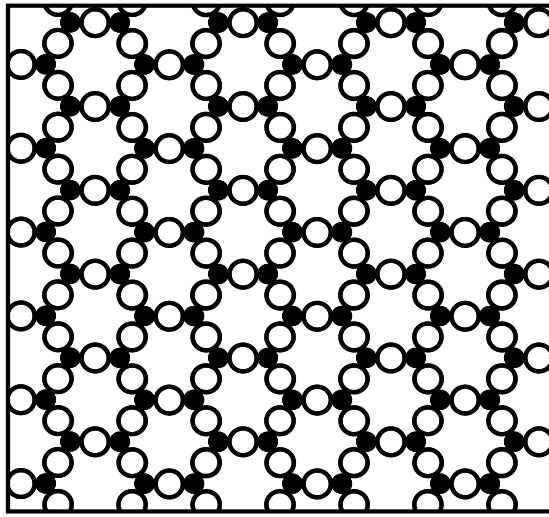
(a) (b)

Figure 4-23 *Two-dimensional schematics give a comparison of (a) a crystalline oxide and (b) a noncrystalline oxide. The noncrystalline material retains short-range order (the triangularly coordinated building block) but loses long-range order (crystallinity). This illustration was also used to define glass in Chapter 1 (Figure 1–8).*
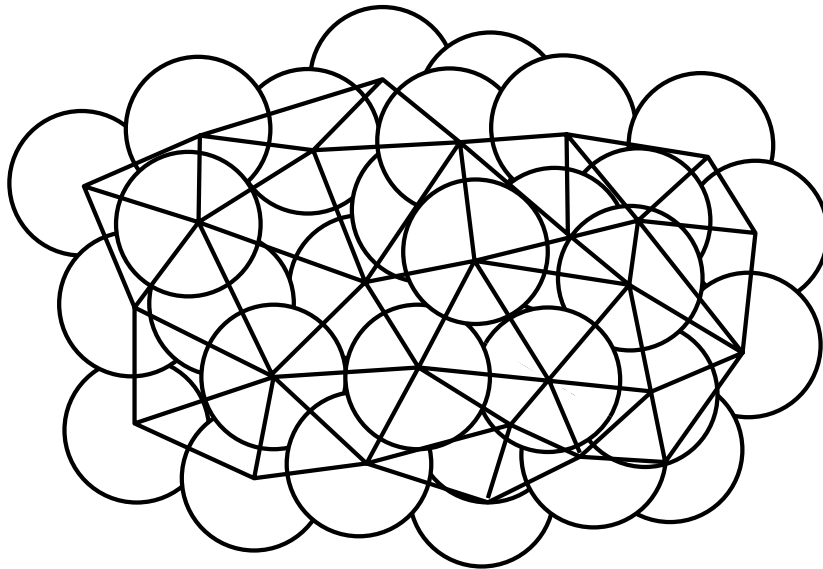
Figure 4-24 *Bernal model of an amorphous metal structure. The irregular stacking of atoms is represented as a connected set of polyhedra. Each polyhedron is produced by drawing lines between the centers of adjacent atoms. Such polyhedra are equivalent to those used to model grain boundary structure in Figure 4–21. In the noncrystalline solid, the polyhedra are not repetitive.*
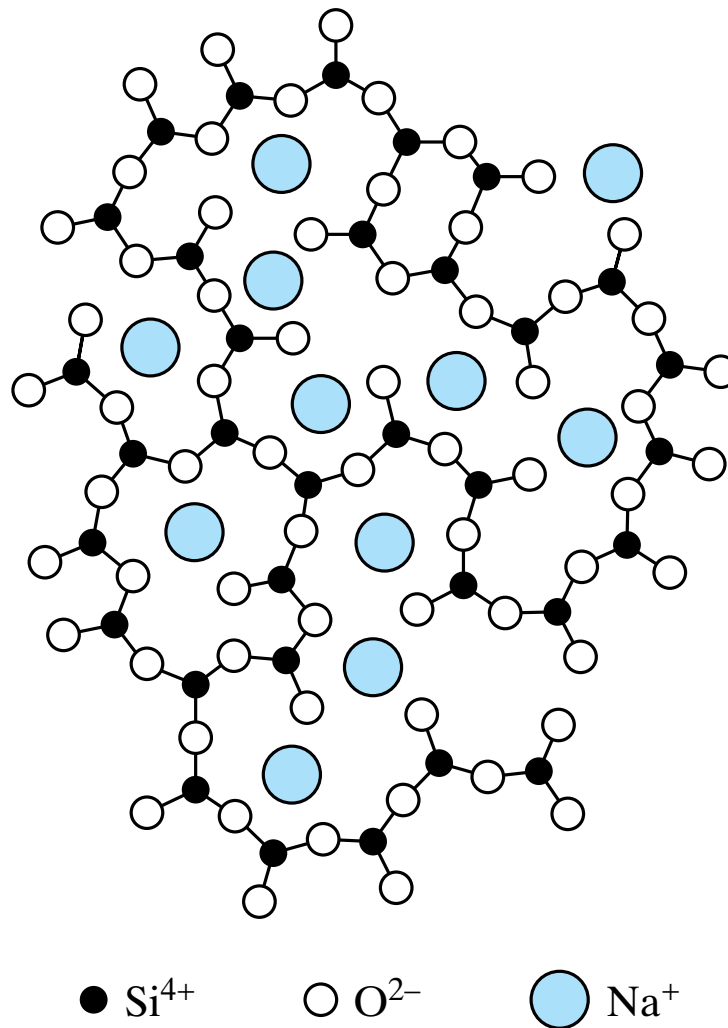
● Si^{4+} ○ O^{2-} Na$^+$

Figure 4-25 *A chemical impurity such as Na$^+$ is a glass modifier, breaking up the random network and leaving nonbridging oxygen ions. [From B. E. Warren,* J. Am. Ceram. Soc. *24, 256 (1941).]*
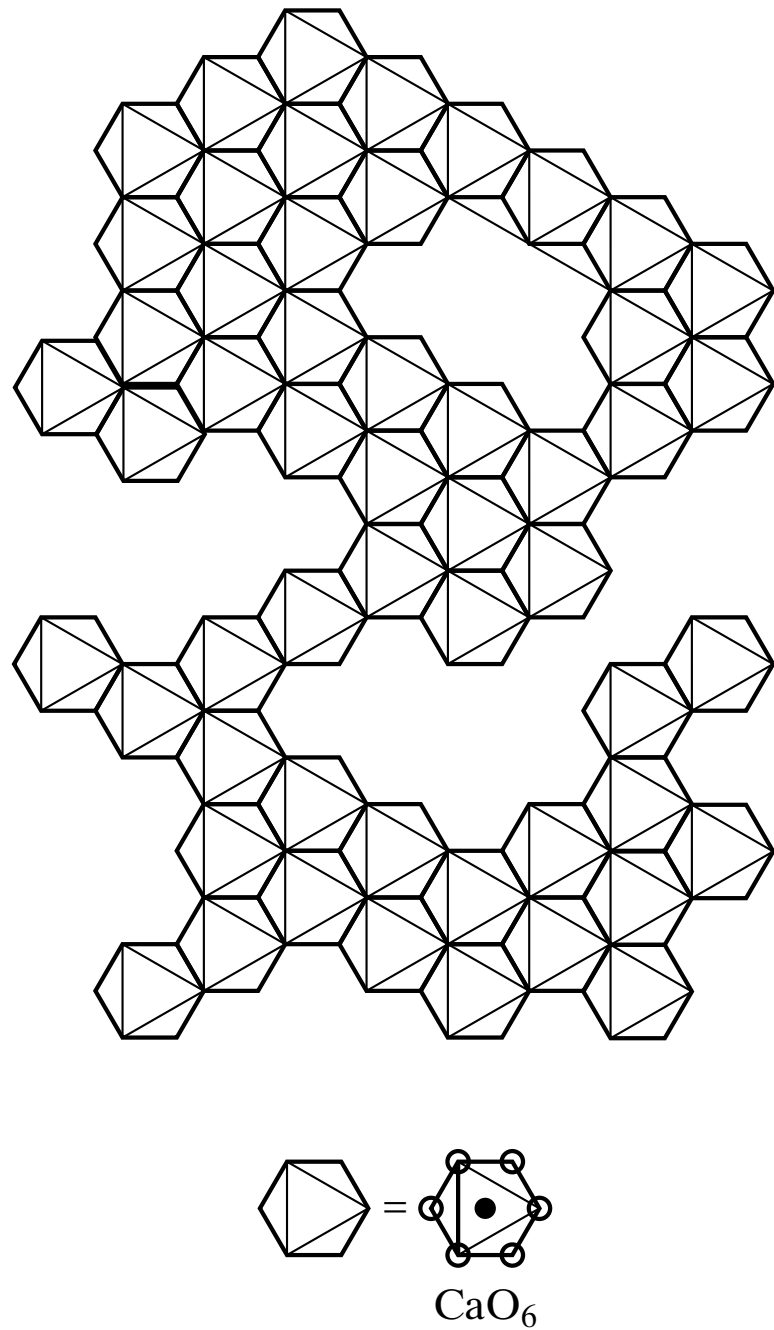
$$CaO_6$$

Figure 4-26 *Schematic illustration of medium-range ordering in a CaO-SiO$_2$ glass. Edge-sharing CaO$_6$ octahedra have been identified by neutron diffraction experiments. [From P. H. Gaskell, et al.,* Nature 350, 675 (1991).]
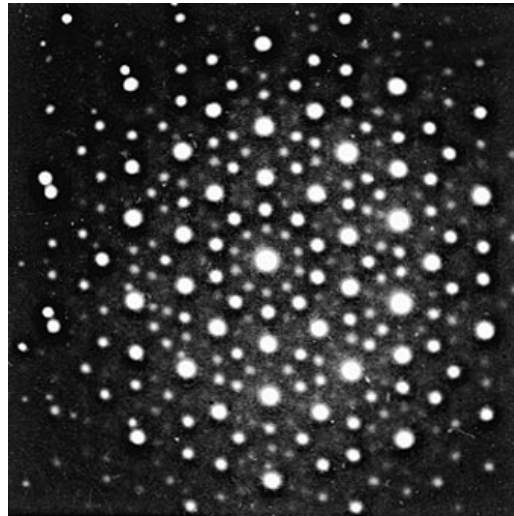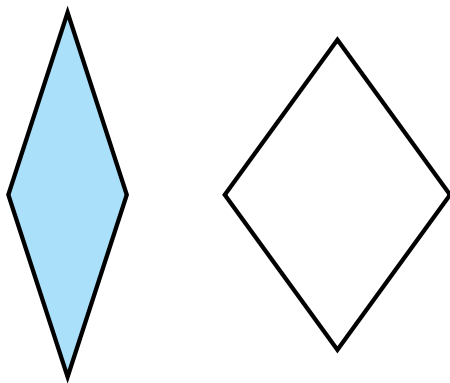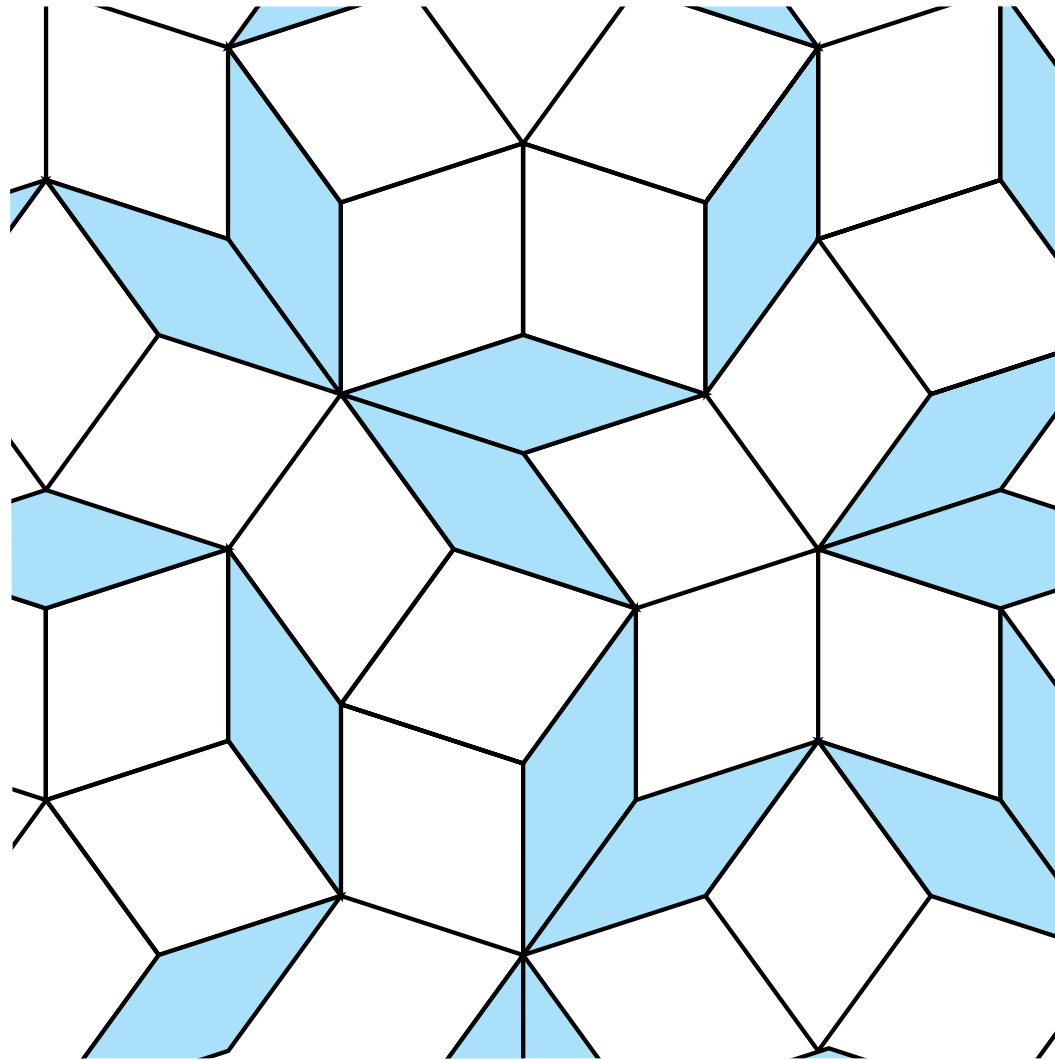
Figure 4-27 *Electron diffraction pattern of a rapidly cooled Al_6Mn alloy showing five-fold symmetry; that is, the pattern is identical with each rotation of 360°/5, or 72°, about its center. Such symmetry is impossible in traditional crystallography. [After D. Schechtman et al.,* Phys. Rev. Letters 53, *1951 (1984).]*

(a)   (b)

Figure 4-28 *(a) Skinny and fat rhombuses can be repeated in (b) a two-dimensional stacking to produce a space-filled pattern with fivefold symmetry. This Penrose tiling provides a schematic explanation for the diffraction pattern of Figure 4–27.*
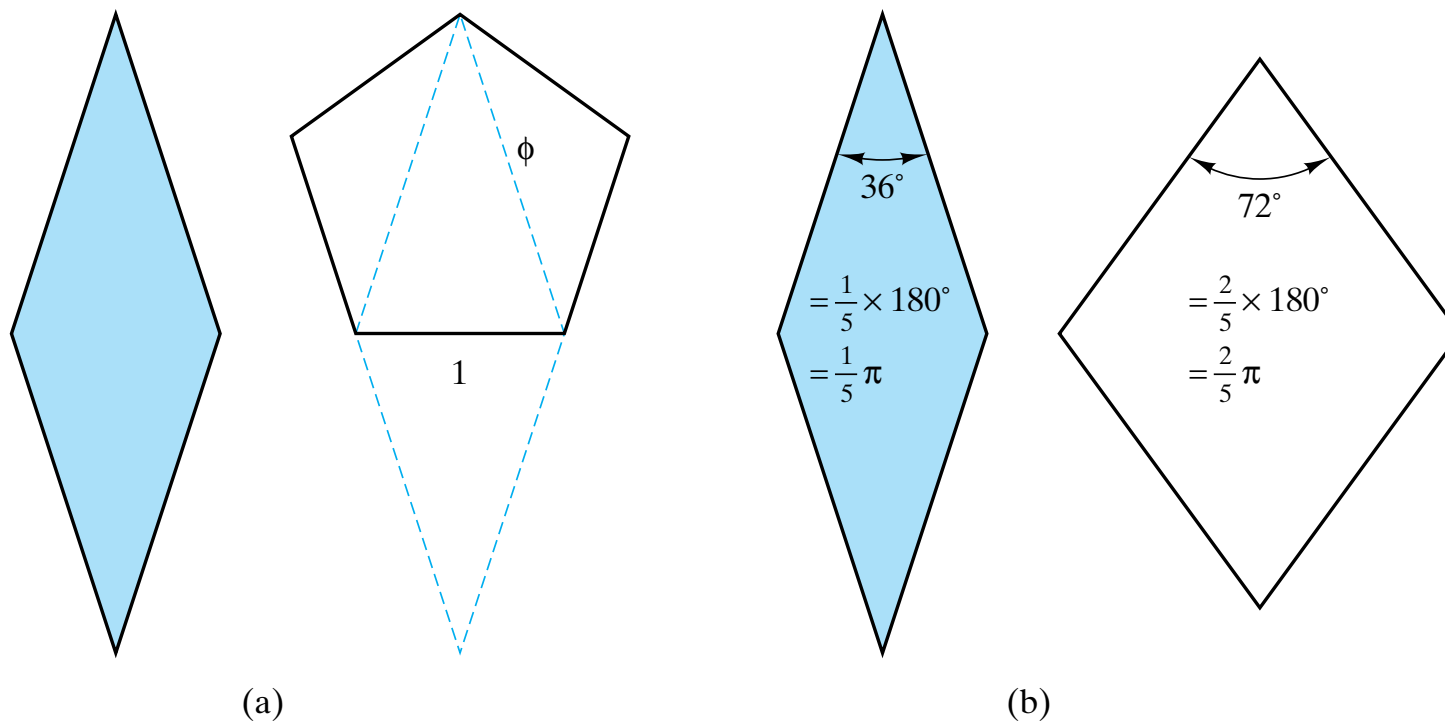
$$\phi$$

$$1$$

$$36°$$

$$= \frac{1}{5} \times 180°$$

$$= \frac{1}{5}\pi$$

$$72°$$

$$= \frac{2}{5} \times 180°$$

$$= \frac{2}{5}\pi$$

(a)   (b)

Figure 4-29 *(a) The relation of the skinny rhombus of Figure 4–28 to the geometry of a regular pentagon. The edge length of the rhombus equals a diagonal of the pentagon, with φ being the golden ratio =* $(\sqrt{5} + 1)/2 = 1.618$*. (b) The acute angle in the skinny rhombus is (1/5)π and, in the fat rhombus, is (2/5)π. These angles assure the fivefold symmetry of the Penrose tiling.*
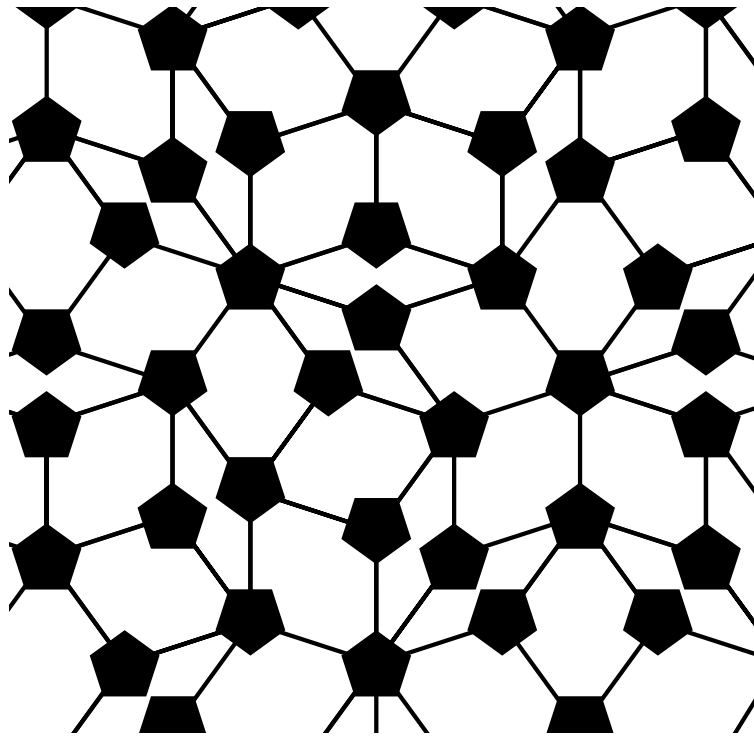
Figure 4-30 *The Penrose tiling of Figure 4–28b decorated with pentagons to illustrate the fivefold symmetry of the overall pattern. Note that there is orientational order (all pentagon bases are parallel), but the lack of regular spacing of pentagons corresponds to a noncrystalline structure.*
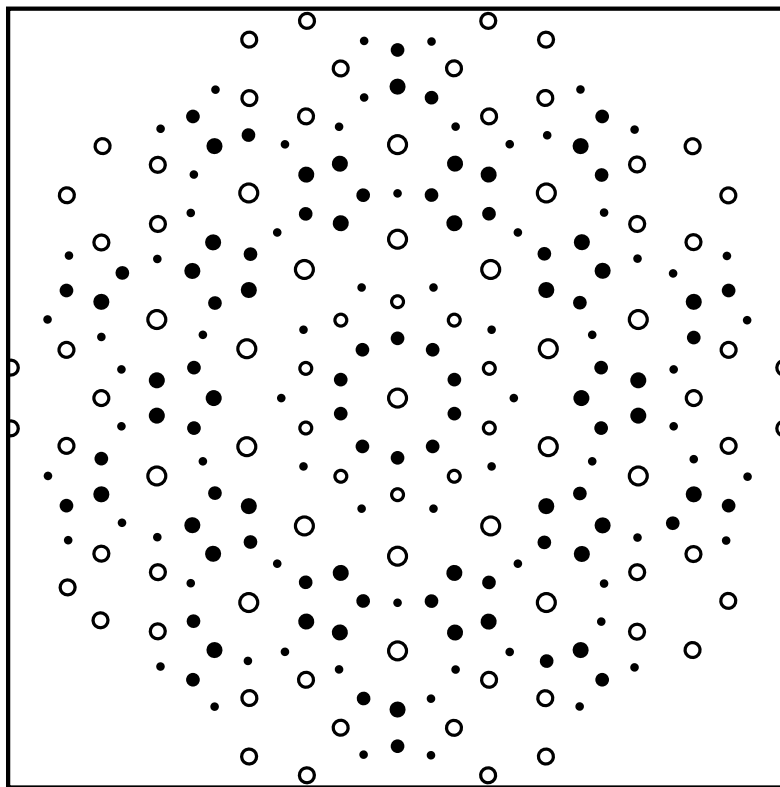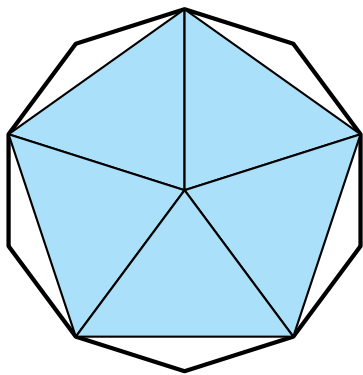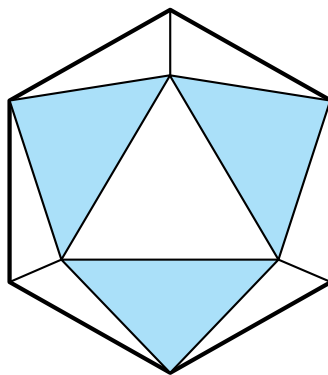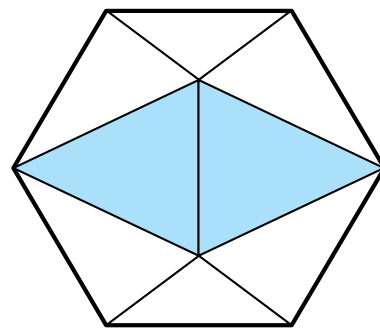
Figure 4-31 *A theoretical diffraction pattern for a three-dimensional Penrose tiling directly matching the experimental pattern of Figure 4–27. [After D. Levine and P. Steinhardt,* Phys. Rev. Letters 53, *2477 (1984).]*

Figure 4-32 *Three views of an icosahedron showing (a) fivefold symmetry, (b) three-fold symmetry, and (c) twofold symmetry.*

Light source

Condenser lens

Objective lens

Projection lens
(eyepiece)

Observation screen
(photographic plate)

(a)

Electron source

Magnetic condenser

Magnetic objective lens

Magnetic projector
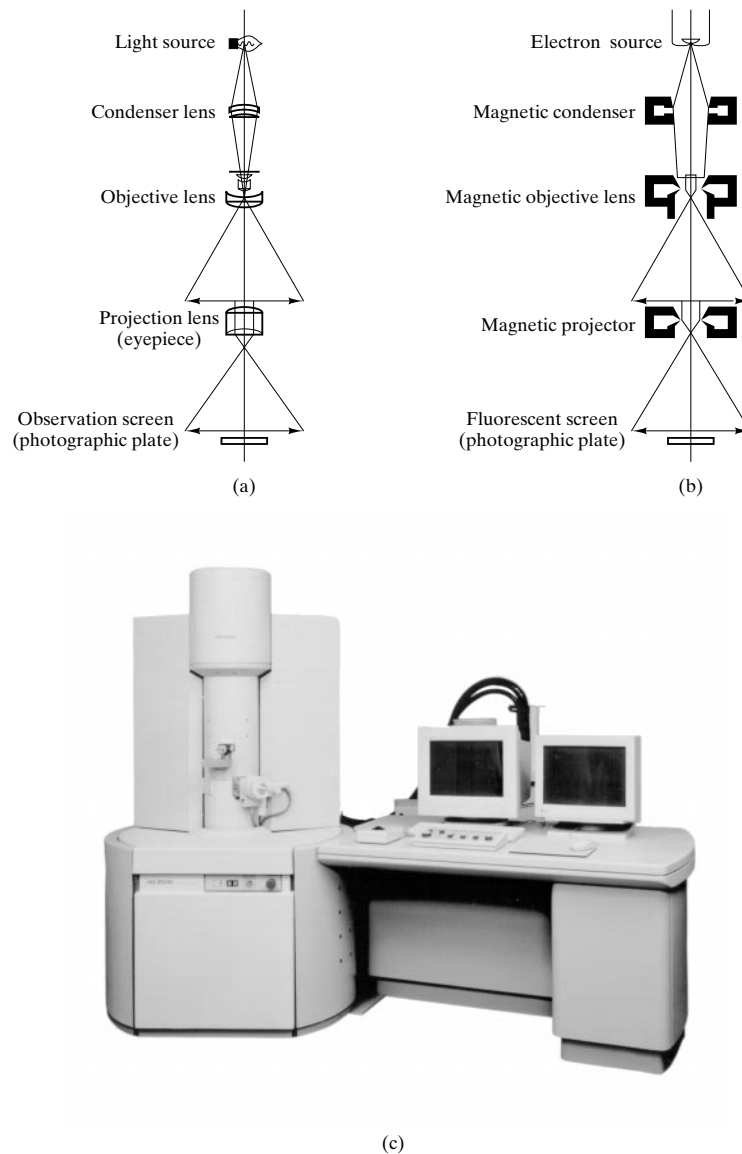
Fluorescent screen
(photographic plate)

(b)

(c)

Figure 4-33 *Similarity in design between (a) an optical microscope and (b) a transmission electron microscope. The electron microscope uses solenoid coils to produce a magnetic lens in place of the glass lens in the optical microscope. (From G. Thomas,* Transmission Electron Microscopy of Metals, *John Wiley & Sons, Inc., New York, 1962.) (c) A commercial TEM. (Courtesy of Hitachi Scientific Instruments.)*
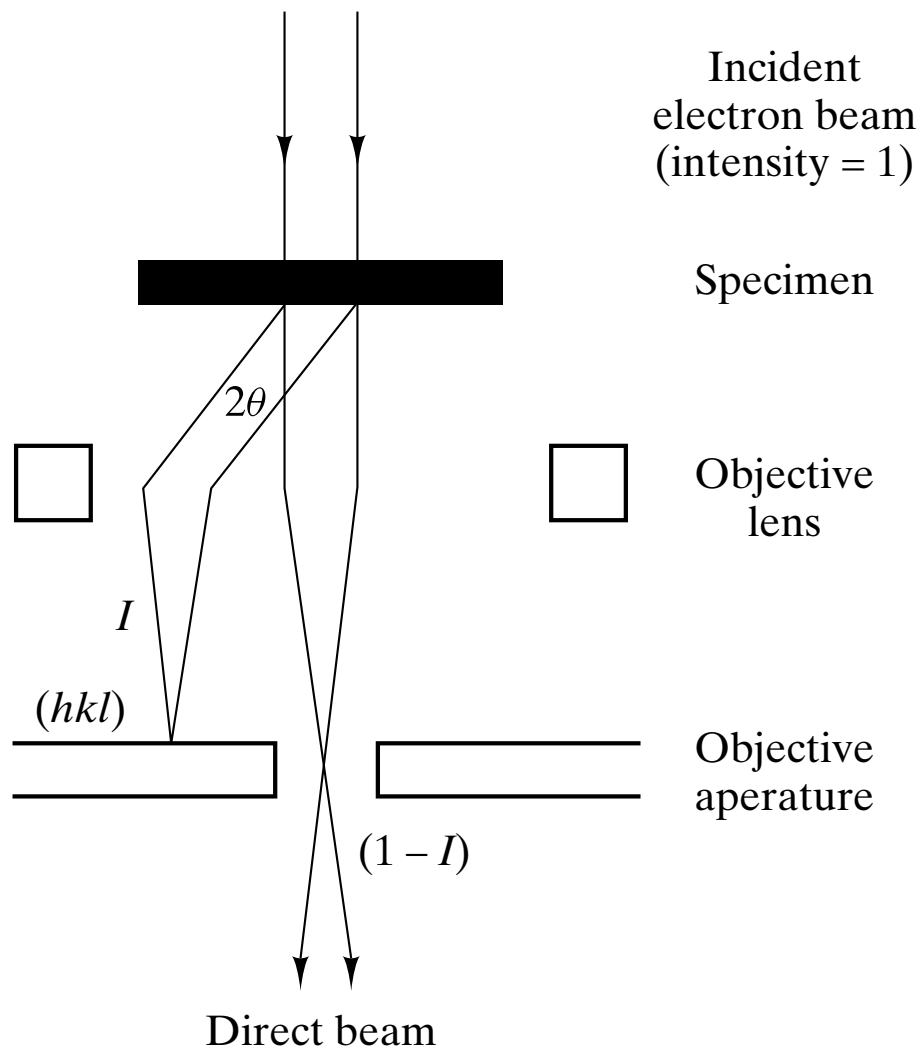
Incident
electron beam
(intensity = 1)

Specimen

2θ

Objective
lens

I

(hkl)

Objective
aperature

$(1 - I)$

Direct beam

Figure 4-34 *The basis of image formation in the TEM is diffraction contrast. Structural variations in the sample cause different fractions (I) of the incident beam to be diffracted out, giving variations in image darkness at a final viewing screen. (From G. Thomas,* Transmission Electron Microscopy of Metals, *John Wiley & Sons, Inc., New York, 1962.)*
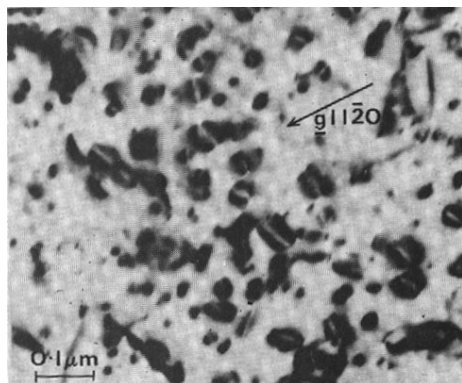
(a)
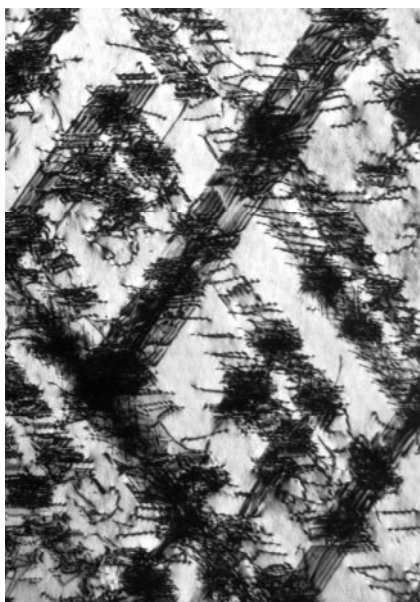
(b)
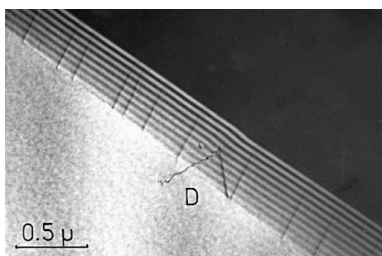
(c)

Figure 4-35 *(a) TEM image of the strain field around small dislocation loops in a zirconium alloy. These loops result from a condensation of point defects (either interstitial atoms or vacancies) after neutron irradiation. (b) Forest of dislocations in a stainless steel as seen by a TEM. (c) TEM image of a grain boundary. The parallel lines identify the boundary. A dislocation intersecting the boundary is labeled "D." [(a) From A. Riley and P. J. Grundy,* Phys. Status Solidi (a) *14, 239 (1972). (b) Courtesy of Chuck Echer, Lawrence Berkeley National Laboratory, National Center for Electron Microscopy. (c) From P. H. Pumphrey and H. Gleiter,* Philos. Mag. *30, 593 (1974).]*

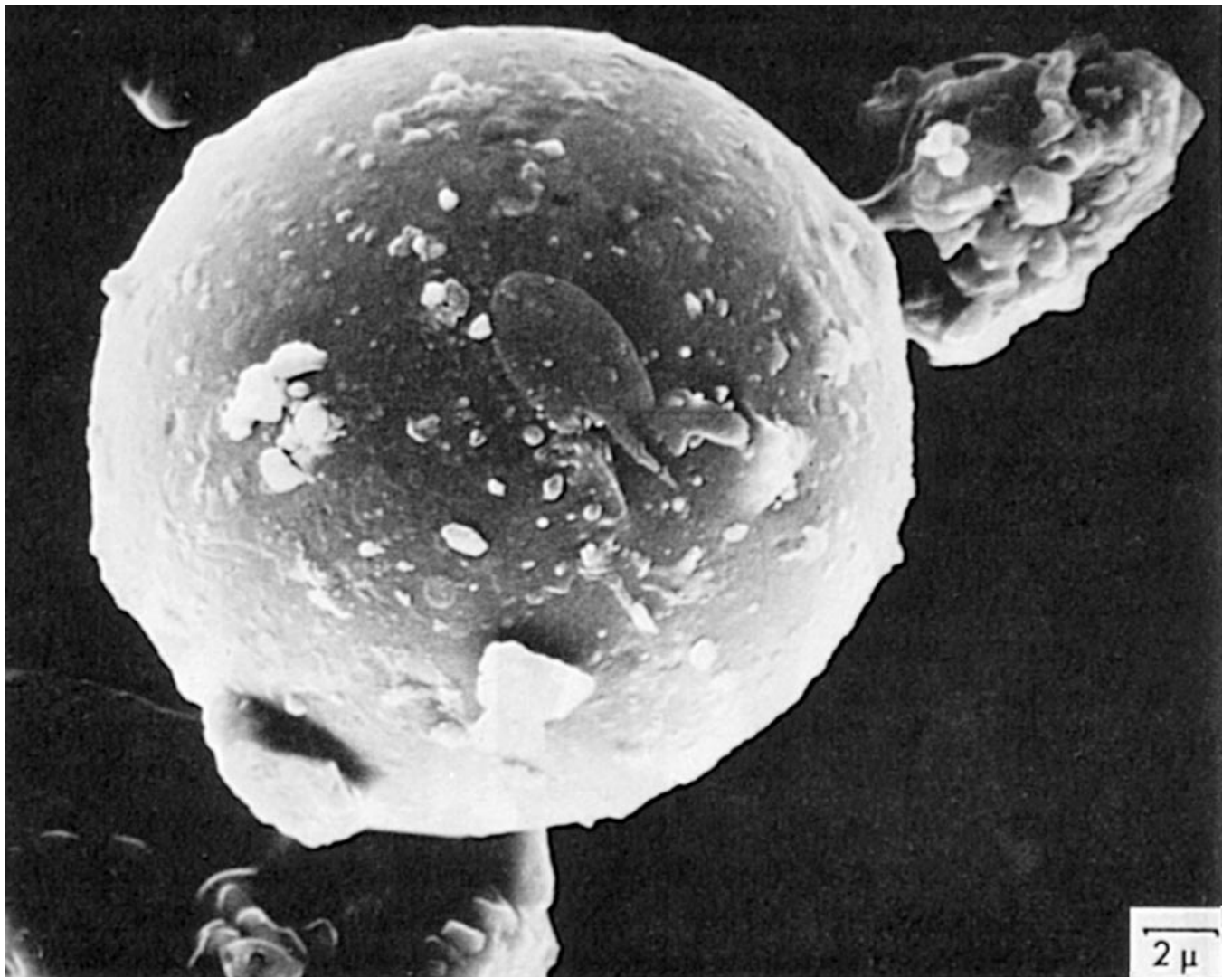Figure 4-36 *A commercial SEM. (Courtesy of Hitachi Scientific Instruments.)*

Figure 4-37 *SEM image of a 23-μm-diameter lunar rock from the Apollo 11 mission. The SEM gives an image with "depth," in contrast to optical micrographs (e.g., Figure 4–18). The spherical shape indicates a prior melting process. (From* V. A. Phillips, Modern Metallographic Techniques and Their Applications, John Wiley & Sons, Inc., New York, 1971.*)*
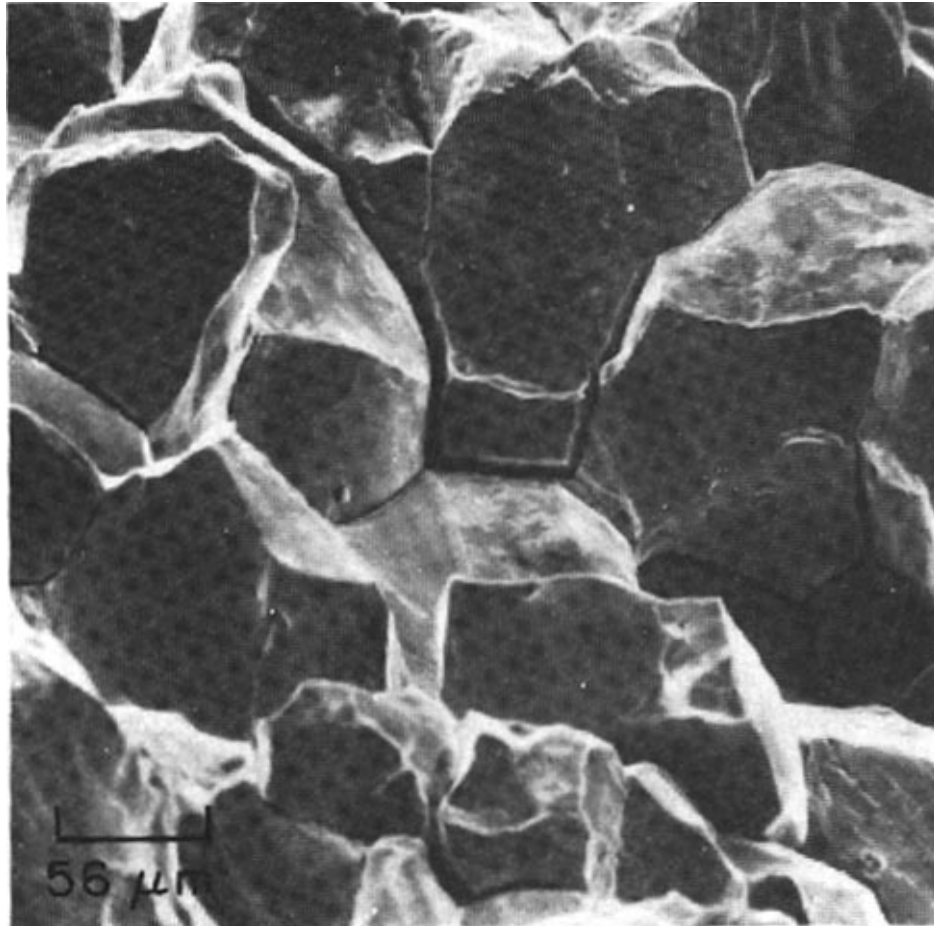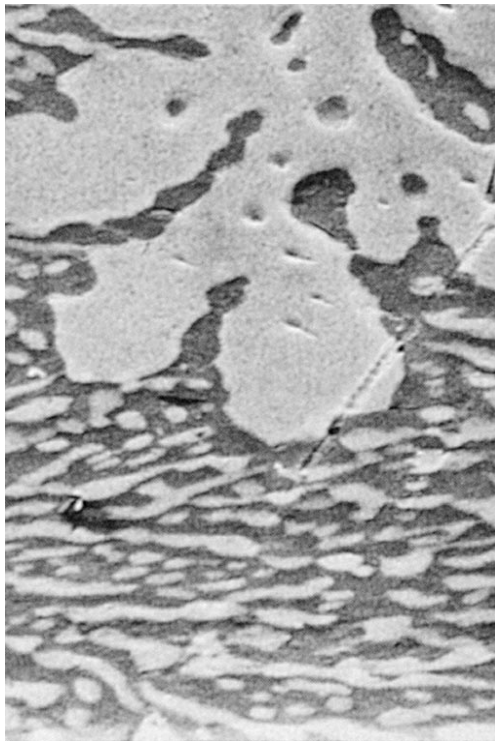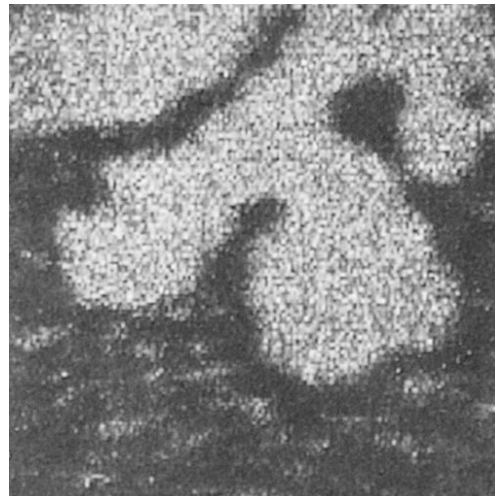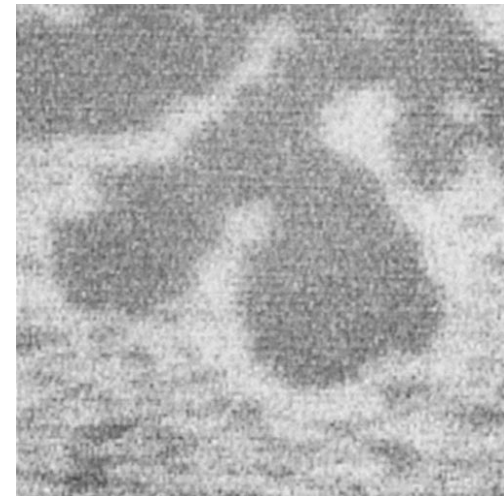
Figure 4-38 *SEM image of a metal (type 304 stainless steel) fracture surface,* 180×*. (From* Metals Handbook, *8th ed., Vol. 9:* Fractography and Atlas of Fractographs, *American Society for Metals, Metals Park, Ohio, 1974.)*

(a)   (b)   (c)

Figure 4-39 *(a) SEM image of the topography of a lead–tin solder alloy with lead-rich and tin-rich regions. (b) A map of the same area shown in (a) indicating the lead distribution (light area) in the microstructure. The light area corresponds to regions emitting characteristic lead x-rays when struck by the scanning electron beam. (c) A similar map of the tin distribution (light area) in the microstructure. [From J. B. Bindell,* Advanced Materials and Processes 143, *20 (1993).]*
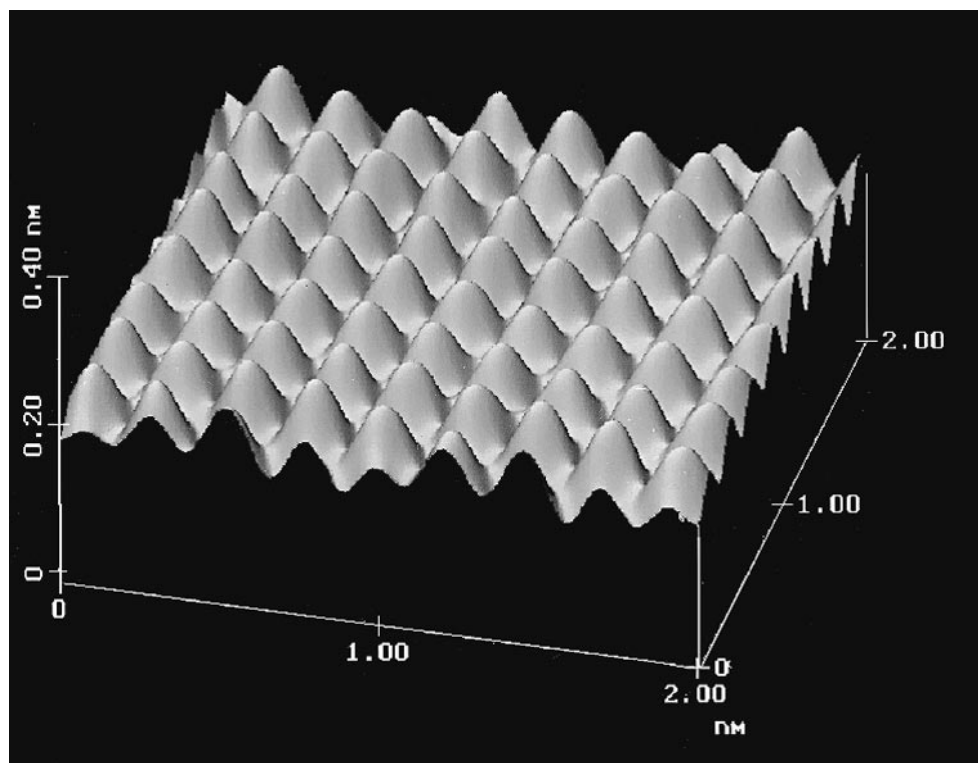
Figure 4-40 *Scanning tunneling micrograph of an interstitial atom defect on the surface of graphite. [From T. L. Altshuler,* Advanced Materials and Processes 140, *18 (1991).]*
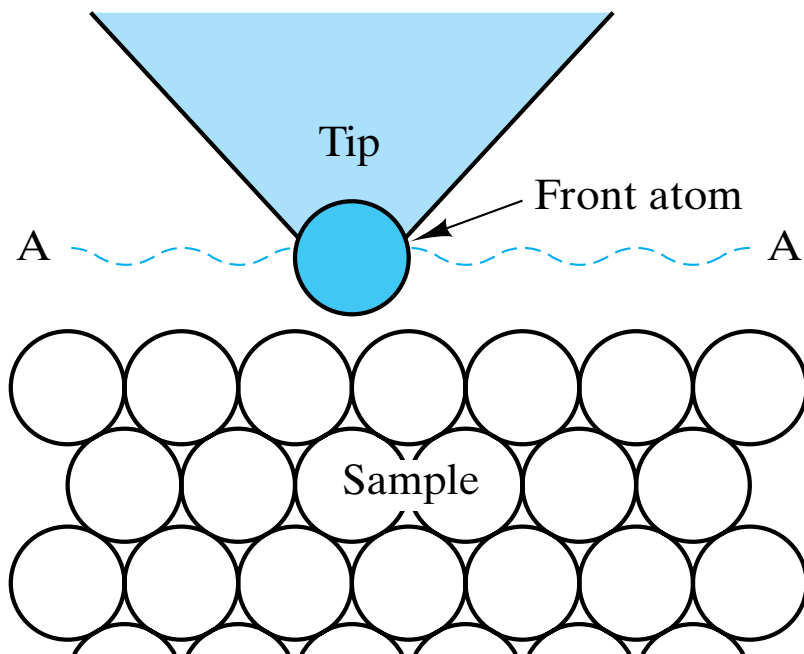
Figure 4-41 *Schematic of the principle by which the probe tip of either a scanning tunneling microscope (STM) or an atomic force microscope (AFM) operates. The sharp tip follows the contour A-A as it maintains either a constant tunneling current (in the STM) or a constant force (in the AFM). The STM requires a conductive sample while the AFM can also inspect insulators.*